Hydrogen Solubility, Interfacial Tension, and Density of the Liquid Organic Hydrogen Carrier System Diphenylmethane/Dicyclohexylmethane

Julius H. Jander,[a] *Patrick S. Schmidt*,[a] *Cédric Giraudet*,[a] *Peter Wasserscheid*,[b,c] *Michael H. Rausch*,*[,a] *Andreas P. Fröba*[a]

[a]Institute of Advanced Optical Technologies − Thermophysical Properties (AOT-TP), Department of Chemical and Biological Engineering (CBI) and Erlangen Graduate School in Advanced Optical Technologies (SAOT), Friedrich-Alexander-University Erlangen-Nürnberg (FAU), Paul-Gordan-Straße 8, 91052 Erlangen, Germany

[b]Institute of Chemical Reaction Engineering (CRT), Department of Chemical and Biological Engineering (CBI), Friedrich-Alexander-University Erlangen-Nürnberg (FAU), Egerlandstraße 3, 91058 Erlangen, Germany

[c]Forschungszentrum Jülich GmbH, Helmholtz Institute Erlangen-Nürnberg for Renewable Energy (IEK-11), Egerlandstraße 3, 91058 Erlangen, Germany

Email addresses: julius.jander@fau.de, patrick.schmidt@fau.de, cedric.giraudet@univ-pau.fr, peter.wasserscheid@fau.de, michael.rausch@fau.de, andreas.p.froeba@fau.de

[*]Author to whom correspondence should be addressed. Tel.: +49-9131-85-25898, fax: +49-9131-85-25878, email: michael.rausch@fau.de, ORCID number: 0000-0003-0719-6758.

Current address of C. Giraudet is: Université de Pau et des Pays de l'Adour, E2S UPPA, CNRS, Total, LFCR, Allée du Parc Montaury, 64600 Anglet, France

ABSTRACT

In the present study, physico-chemical properties of the liquid organic hydrogen carrier (LOHC) system diphenylmethane/dicyclohexylmethane in the presence of dissolved hydrogen are presented for temperatures up to 523 K and pressures up to 10 MPa. Solubility of hydrogen, interfacial tension, and liquid density were measured by the isochoric saturation method, the pendant-drop method, and vibrating-tube method, respectively, which are realized in two experimental setups. The solubility of hydrogen increases with increasing temperature and pressure. For the fully hydrogenated dicyclohexylmethane, it is about 50% higher than for the non-hydrogenated diphenylmethane and similar to that of a mixture from a deliberately stopped hydrogenation process containing also partially hydrogenated cyclohexylphenylmethane. While the interfacial tension decreases slightly with increasing hydrogen pressure at constant temperature, the density remains approximately constant. The latter properties obtained for different mixtures with similar degree of hydrogenation show that the influence of the presence of cyclohexylphenylmethane is small.

KEYWORDS - density, dissolved hydrogen, interfacial tension, LOHC systems, solubility

ABBREVIATIONS

AARD	average absolute relative deviation
Ar	argon
DoH	degree of hydrogenation
EoS	equation of state
GC-FID	gas chromatography with coupled flame-ionization detection
GC-MS	gas chromatography with coupled mass spectroscopy
H_2	hydrogen
H0-BT	benzyltoluene
H12-BT	perhydrobenzyltoluene
H0-DBT	dibenzyltoluene
H18-DBT	perhydrodibenzyltoluene
H0-DPM	diphenylmethane
H6-DPM	cyclohexylphenylmethane
H12-DPM	dicyclohexylmethane
H0-NEC	N-ethylcarbazole
H12-NEC	perhydro-N-ethylcarbazole
HFE-7300	1,1,1,2,2,3,4,5,5,5-decafluoro-3-methoxy-4-(trifluoromethyl)-pentane
LOHC	liquid organic hydrogen carrier
PEEK	polyether ether ketone
RMS	root mean square
SLS	surface light scattering
VLE	vapor-liquid equilibrium

1. Introduction

In an economy based on renewable energy resources, fluctuations in electricity production by, *e.g.*, wind and solar power, have to be compensated by suitable energy storage technologies to align power generation and demand [1–5]. Hydrogen (H_2) is considered as a promising energy carrier for this purpose, but its storage in pure form is challenging regarding safety, efficiency, and transportation aspects [2,4–7]. A currently discussed option for efficient and infrastructure-compatible logistics of H_2 is the Liquid Organic Hydrogen Carrier (LOHC) technology [2-4,6-9]. This technology uses reversible hydrogenation/dehydrogenation cycles and enables safe storage of H_2. The H_2-lean LOHC compounds are typically aromatic or heteroaromatic liquids [6,10]. For the effective design of optimized devices for LOHC-based H_2 storage processes, reliable thermophysical property data such as liquid density, interfacial tension, and H_2 solubility are crucial. For instance, solubility data for H_2 in the LOHC components and mixtures represent essential information for the design of hydrogenation and dehydrogenation reaction equipment [11]. Furthermore, interfacial tension influences catalyst wetting [12], while the liquid density is related to the volumetric H_2 storage density which is an important performance indicator of LOHC systems [2,4,7].

The availability of the corresponding data for relevant LOHC systems is, however, limited so far. This holds in particular true for process-relevant conditions that cover temperatures T up to 673 K and pressures p up to 7 MPa [6,13] and include the presence of H_2. The published experimental investigations of the H_2 solubility in LOHC components have covered the N-ethylcarbazole (H0-NEC)/perhydro-N-ethylcarbazole (H12-NEC) [14], dibenzyltoluene (H0-DBT)/perhydrodibenzyltoluene (H18-DBT) [14,15],

toluene/methylcyclohexane [14,16–18], and benzene/cyclohexane [16,18] systems at *T* up to 373 K and *p* up to about 10 MPa. In all these studies, H_2 was found to exhibit a higher solubility in the hydrogenated LOHC compounds. Regarding liquid density and interfacial tension, all published experimental studies were performed in absence of H_2. They provide *T*-dependent data at ambient or saturation pressure for the H0-NEC/H12-NEC [19], H0-DBT/H18-DBT [20-22], benzyltoluene (H0-BT)/perhydrobenzyltoluene (H12-BT) [20], benzene/cyclohexane [23–26], and toluene/methylcyclohexane [24,25,27–29] LOHC systems. In addition, *p*-dependent liquid-density data are available for the pure compounds of the toluene/methylcyclohexane LOHC system [30–32], but not for the NEC-, DBT-, and BT-based systems.

In recent years, the DBT- and BT-based LOHC systems [13,21,33] and corresponding mixtures [34] have gained attention due to their high thermal stabilities, excellent technical availability, considerable H_2 loading capacity, and low melting points. These systems are applied as mixtures of their regioisomers. This accounts for their low melting points, but complicates conclusions regarding the influence of structural features on their physico-chemical properties. It is, therefore, of high fundamental interest to investigate structural analogues which may have slightly higher melting points, but represent pure compounds. For this reason, we have chosen the LOHC system diphenylmethane (H0-DPM)/dicyclohexylmethane (H12-DPM) as such a highly interesting reference LOHC system for our recent study [35]. Moreover, this system is of considerable technical interest. It is characterized by a higher mass-based H_2 storage capacity compared to, e.g., the DBT-based LOHC system (6.7 mass% H_2 compared to 6.2 mass% H_2) and by a lower viscosity of H12-DPM compared to H18-DBT [21,35]. The volumetric H_2 storage capacity of H12-DPM is 58.5 kg_{H2}/m^3 at p = 0.1 MPa and T = 298.15 K [35]. Considering pure H_2 storage options discussed for mobility applications [36], this capacity is higher than that of

compressed H_2 (39.2 kg_{H2}/m^3 at p = 70 MPa, T = 298.15 K [37]) and lower than that of liquefied H_2 (70.9 kg_{H2}/m^3 at p = 0.1 MPa, $T_{saturation}$ = 20.32 K [37]). The acute toxicity of H0-DPM is low, but its aquatic toxicity is significant [38]. For H12-DPM, no information on toxicity could be found, which reflects the need for comprehensive hazard assessment for LOHCs expressed by Rao and Yoon [10]. A viable option for the major practical drawback of the H0-DPM/H12-DPM LOHC system, which is the comparatively high melting point of H0-DPM of about 295 K [38], is the application of mixtures with H12-DPM [35] or biphenyl [39-41].

Until recently, literature data on the physico-chemical properties of the H0-DPM/H12-DPM LOHC system have only existed for pure H0-DPM in form of density data in the compressed liquid phase at p up to 30 MPa [42], interfacial tension at ambient p [43,44] as well as H_2 solubility up to T = 702 K and p = 25 MPa [45,46]. These data have been extended by some of us in our previous study of the liquid density of H0-DPM and H12-DPM at p = 0.1 MPa as well as their interfacial tensions and viscosities at $p \approx 0.1$ MPa in argon atmosphere in a T range from (303 to 593) K [35].

In the present study, the H_2 solubility as well as the influence of the presence of H_2 on the liquid density ρ' and the interfacial tension σ were investigated for H0-DPM and H12-DPM. Additionally, a technical mixture originating from a hydrogenation process of H0-DPM with a degree of hydrogenation of 0.551 containing also the partially hydrogenated intermediate cyclohexylphenylmethane (H6-DPM) and a binary mixture of H0-DPM and H12-DPM of the same degree of hydrogenation were examined. By this, also the influence of the presence of H6-DPM on σ and ρ' was checked. For these investigations, two experimental setups were designed, validated, and applied.

2. Experimental section

***2.1 Materials and sample preparation*.** Information about the used liquid samples and gases as well as their purities and mixture compositions in terms of mass fraction w or molar fraction x is summarized in Table 1. Three samples of H12-DPM were produced by catalytic hydrogenation of purchased H0-DPM in individual hydrogenation runs. Using gas chromatography with coupled mass spectroscopy (GC-MS) and gas chromatography with coupled flame ionization detection (GC-FID) for analysis, H0-DPM was found to correspond to the specifications stated by the manufacturer, while the synthesized H12-DPM samples, further referred to as A, B, and C, had purities of w = (0.998, 0.975, and 0.990), respectively. The impurities in the H12-DPM samples were found to consist of H0-DPM, the partially hydrogenated intermediate H6-DPM, and a residual fraction of other components. In the following, it is indicated which H12-DPM sample was used for the respective measurements. The slight differences of the H12-DPM samples under investigation are also considered in our discussion. The investigated technical LOHC mixture, consisting of H0-DPM, H6-DPM, and H12-DPM, originated from a deliberately stopped hydrogenation experiment of H0-DPM and is referred to as ‘reaction mixture’ in the following. A degree of hydrogenation (DoH) of 0.551 was determined for this mixture by considering the respective hydrogen contents of the individual LOHC compounds and their respective quantities in the mixture. The DoH is defined as the fraction of the number of hydrogen atoms bound to an LOHC molecule by the hydrogenation reaction compared to its maximum molar uptake capacity [34]. An absolute uncertainty of 0.002 for the determined DoH values results from the evaluation of the mixture composition by GC-FID. The impurity mass fraction $w_{\mathrm{impurities}}$ = 0.002 related to all mixture components can be assigned to substances possibly representing partially hydrogenated products. As these compounds cannot be quantified

accurately and their impact on the DoH is smaller than its uncertainty, they are not considered in the determination of the DoH. To reproduce the DoH of the reaction mixture in a binary mixture of H0-DPM and H12-DPM, appropriate amounts of these compounds were weighed using a balance with a digit precision of 0.1 mg and an estimated expanded uncertainty (k = 2) of 1 mg. In the preparation procedure of the two binary mixtures using the H12-DPM samples A or B, the impurities were also not considered. Thus, the finally determined and reported DoH of the binary mixtures considering only the contributions of H0-DPM and H12-DPM was slightly smaller than targeted especially for the one prepared with the H12-DPM sample B of lower purity.

Table 1 - Specification of used samples.

Substance	CAS number	Source	Molar mass M ($g \cdot mol^{-1}$)	Specified / measured purity or mixture composition / DoH
H0-DPM	101-81-5	Sigma Aldrich	168.23	$w = 0.999^{a,b}$
H12-DPM	3178-23-2	Self-made	180.33	$w = 0.998^{b}$ (A) $w = 0.975^{b}$ (B) $w = 0.990^{b}$ (C)
Binary mixture with H12-DPM (A)		Self-made		$w_{impurities} = 0.002^{c}$ $x_{H0\text{-}DPM} = 0.449^{c}$ $x_{H12\text{-}DPM} = 0.551^{c}$ DoH = 0.551 ± 0.002
Binary mixture with H12-DPM (B)		Self-made		$w_{impurities} = 0.015^{c}$ $x_{H0\text{-}DPM} = 0.455^{c}$ $x_{H12\text{-}DPM} = 0.545^{c}$ DoH = 0.545 ± 0.002
Reaction mixture		Self-made		$w_{impurities} = 0.002^{b}$ $x_{H0\text{-}DPM} = 0.098^{d}$ $x_{H6\text{-}DPM} = 0.702^{d}$ $x_{H12\text{-}DPM} = 0.200^{d}$ DoH = 0.551 ± 0.002

Hydrogen	1333-74-0	Linde AG	2.016	$x = 0.999999^{a}$
Argon	7440-37-1	Linde AG	39.948	$x = 0.99999^{a}$

[a]Purity as specified by the manufacturer in the certificate of analysis for the used batch.
[b]Purity measured using GC-FID analysis.
[c]Calculated from compositions measured for used H0-DPM and H12-DPM samples and their masses.
[d]Mole fraction of main components excluding impurities as measured using GC-FID analysis and used to determine DoH.

In the preparation of the binary samples from H0-DPM and H12-DPM, traces of H6-DPM in the H12-DPM were treated as impurities and were not included in the corresponding DoH calculations. Argon (Ar) was used as inert gas atmosphere for interfacial tension measurements without H_2 and in the sample flasks during storage. All substances were used without further purification.

2.2 Density – Vibrating-tube method. Liquid density measurements of the LOHC samples at ambient air atmosphere were performed by using the vibrating-tube densimeters DMA 5000 M and 4200 M from Anton Paar for T from (283.15 to 473.15) K. The latter instrument has been calibrated for measurements with varying p according to the physically-based approach of May et al. [47] and was also integrated in the setup dedicated to solubility measurements. There, it was used to measure the densities of the compressed liquid phase of the H_2-free LOHC samples in a T range from (293.15 to 473.15) K in steps of 25 K at p of (3, 7, and 10) MPa as well as of the LOHCs close to their saturation with dissolved H_2 at $T \approx$ (323, 373, 423, and 473) K in a p range from (1 to 10) MPa. Detailed information on all corresponding measurement procedures, processing of measurement data, and the resulting uncertainties is given in section S1 of the Supporting Information.

2.3 Solubility – Isochoric-saturation method. The solubility of H_2 in the DPM-based LOHC compounds was investigated by the isochoric-saturation method [48] using a new apparatus. A schematic representation of the setup is given in Figure 1. It consists of three major parts, which are the vapor-liquid equilibrium (VLE) cell, a circulation loop for the liquid phase, and a manifold for gas handling. The VLE is established in the *T*-controlled VLE cell, which is made of H_2-resistant stainless steel and possesses two opposing sapphire windows. The cell exhibits a specified inner volume of 0.17 L and can be operated up to T = 573 K and p = 50 MPa. The T control of the cell is realized by resistance heating, based on T measured in the cell wall close to its outer surface. For measuring T related to the liquid and the gas phase as well as in the vicinity of an optical window, three additional T probes are located in the cell wall as close as possible to the zones of interest. p inside the VLE cell is measured by a pressure transducer. To expedite the dissolving process of the gas in the liquid phase, a controllable electrical stirrer is integrated in the sample cell. The circulation loop for the liquid phase allows measurements of the liquid-phase density ρ' using the integrated densimeter DMA 4200 M at T up to 473 K and p up to 40 MPa. The liquid is circulated by a centrifugal pump with small pressure gradient and low pulsation to minimize disturbance of the VLE. Coming from the bottom of the VLE cell, the liquid flow is guided through a screw pump and the densimeter before being returned to the VLE cell. The densimeter and the screw pump can be isolated from the remaining system for ρ' measurements of the pure LOHC sample under pressure before adding gas, where p is adjusted by operation of the screw pump and measured by a further pressure transducer. T of the screw pump and the pump head are controlled by resistance heating, using inserted probes for corresponding T measurements. With the manifold for gas handling, the complete apparatus can be evacuated, filled, and pressurized with gas.

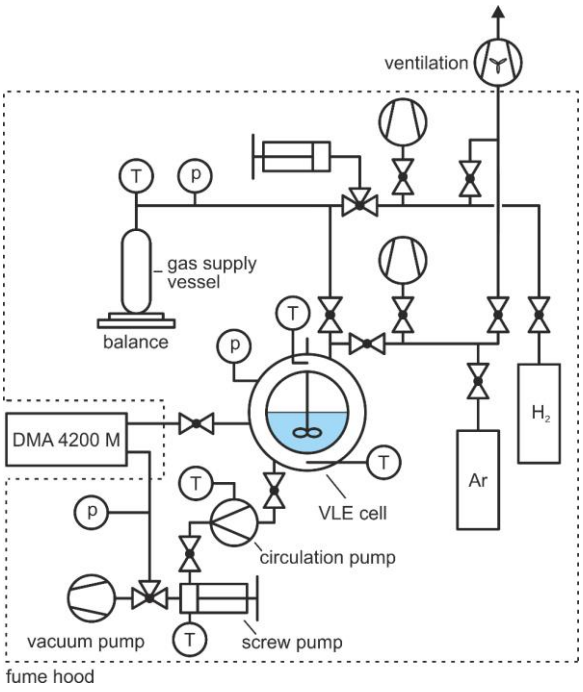

Figure 1 - Schematic representation of the new experimental apparatus for determination of H_2 solubility in LOHC compounds as well as density of the gas-saturated and the pure compressed liquid. (designed for single column, color only in online publication)

The investigated gas is contained in a stainless-steel gas-supply vessel with an inner volume of about 0.15 L, from which the gas can be dosed to the VLE cell. The vessel can be charged with gas up to p = 25 MPa by a screw pump. T of the gas in the reservoir is measured directly in the vessel, while the gas pressure is measured in the connected manifold. The amount of gas injected into the gas-phase volume of the established VLE can be evaluated using both gravimetry and equations of state (EoS). For determining the mass difference in the gas-supply vessel when applying gravimetry, the vessel is placed on a balance providing a digit precision of 1 mg. To ensure mechanical decoupling of the weighed vessel, its connection to the manifold system is given by a flexible capillary tube made of polyether ether ketone (PEEK). All T measurements are conducted by using Pt100 resistance probes calibrated to an absolute

uncertainty (k = 2) of 0.02 K. The pressure measurements are performed using calibrated pressure transducers with absolute uncertainties (k = 2) of 0.015 MPa.

For the evaluation of the solubility, the total volumes of the VLE cell, the liquid circulation loop, and the gas supply vessel including its connection to the VLE cell were calibrated with an estimated expanded relative uncertainty (k = 2) of about 0.35% according to the procedure explained in section S2a of the Supporting Information.

Before each measurement series, all components of the VLE cell and the liquid circulation line were thoroughly cleaned. After evacuation of the complete setup, the VLE cell was filled with Ar while being decoupled from the liquid circulation loop. Between (80 and 140) g of the liquid sample was filled stepwise into the VLE cell, where the total sample mass was determined by weighing the used syringe before and after each filling step using a balance with a digit precision of 0.1 mg and an estimated expanded uncertainty (k = 2) of 1 mg. Then, the VLE cell was evacuated for a short time and supplied with Ar at p = 0.2 MPa. The bottom valve of the VLE cell was opened to fill the evacuated circulation line including the densimeter with liquid. After closing the valve, the liquid-phase density of the pure sample was measured as a function of T and p according to the procedure described in section S1b of the Supporting Information. Before being pressurized with H_2 from the gas supply vessel, the VLE cell was evacuated close to the vapor pressure of the investigated liquid for a short time. During the following operation of the setup, T and p were continuously monitored. The pump and the stirrer were switched on for at least 2 h to establish VLE for each state point. As soon as T and p in the VLE cell and the oscillation period of the densimeter had stabilized, the stirrer and the circulation pump were switched off. T and p data recorded during 2 min after about 30 min of further equilibration were used for data evaluation. Here, the average of T measured close to the gas and the liquid phase in

the VLE cell as well as the average of p measured in the VLE cell and the liquid circulation loop were considered. In the following statements, the first value always represents the average for the considered system and T range, whereas the corresponding maximum is given in brackets. The difference between the aforementioned temperatures was 0.123 (0.406) K for T < 380 K and 0.867 (1.40) K for T > 380 K for all systems. The increasing difference with increasing T is associated with the necessary cooling of the magnetic coupling in the installed stirrer. For H12-DPM, the stability of the individual T probes was better than ±3.8 (±12.4) mK and ±5.9 (±26.4) mK in the same T ranges as given above, whereas for H0-DPM and the reaction mixture, stabilities better than ±0.9 (±1.7) mK and ±0.9 (±1.9) mK, respectively, were achieved. To describe the stability of p measured with the two transducers, the double standard deviation is reported, which is smaller than 0.61 (1.2) kPa for H12-DPM for T > 380 K and smaller than 0.4 (0.6) kPa for all other systems and state points. The p values measured with the individual transducers always agreed with the reported average within their expanded uncertainty (k = 2) of $U(p)$ = 15 kPa.

Due to the small density of H_2, its injected mass was calculated based on the measured p- and T-differences in the gas supply vessel before and after each injection step. For that, the corresponding density data obtained from the EoS of Leachman et al. [49] implemented in the NIST Standard Reference Database REFPROP [37] and the calibrated volume of the gas supply vessel and its connection line to the VLE cell were considered. The small leakage mass flow of H_2 from the VLE cell caused by diffusion through the gaskets being on average 0.16 $mg \cdot h^{-1}$ was considered for the complete experimental time. It was estimated for each individual stabilized state point based on the slight, linear decrease in gas density during the corresponding data acquisition period.

For each state point, the mass of LOHC and H_2 being present in the VLE cell and the circulation loop, the average *T* and *p* data, and the liquid density with dissolved H_2 at this state point determined according to section S1c of the Supporting Information were considered in iteration calculations. These are necessary because the volumes of the liquid and the gas phase are not exactly known. In the first iteration, the liquid volume is estimated using the mass of the filled LOHC and the aforementioned liquid density. Knowledge of the calibrated overall volume allows the calculation of the volume of the gas phase. The partial pressure of H_2 therein is determined by subtracting the vapor pressure of the LOHC from the measured average total pressure *p*. Vapor pressures were obtained from available data for H0-DPM [50] and H12-DPM [51–53]. The vapor pressure of H6-DPM was estimated by the arithmetic mean of the vapor pressures of H0-DPM and H12-DPM. The vapor pressures of the mixtures were estimated by mole fraction-weighted combination of the vapor pressures of the pure compounds. Assuming an ideal gas, the vapor pressure of the LOHC and the gas-phase volume are used to calculate the mass of LOHC therein. With the partial pressure of H_2, its partial density at the measured *T* was calculated using the EoS of Leachman et al. [49] and combined with the gas-phase volume to obtain the mass of H_2 in the gas phase. Considering the masses of H_2 injected into the VLE system, lost through the gaskets until the evaluated state point was reached, and being present in the gas phase, the mass of H_2 dissolved in the liquid phase is determined. These results allow recalculation of the mass and, thus, the volume of the liquid phase, which represents the start of the second iteration. At least three iterations were performed until convergence of the final value for the mass of dissolved H_2 was found. The relative change in dissolved H_2 mass for the last iteration compared to the previous value was always smaller than 0.006%. Based on the

determined masses of LOHC and H_2 in the liquid phase, the corresponding mole fraction x_s of dissolved H_2 representing its solubility is determined.

To estimate the uncertainty of the x_s results, error propagation calculations in quadrature were applied considering all input uncertainties in the final iteration. The initial input uncertainties are related to the mass of filled LOHC, the calibrated internal volumes of the apparatus parts, the liquid density of the LOHC with dissolved H_2 as well as the measured T and p data. The latter uncertainties are used for worst-case estimations of the uncertainty of the gaseous H_2 density data determined by the EoS of Leachman et al. [49], which exceed the uncertainty inherent in the EoS. For the leakage mass flows of H_2 and the vapor densities of the LOHCs, an expanded relative uncertainty (k = 2) of 10% was estimated.

For validation of the experimental setup and the evaluation procedure, solubility measurements were successfully performed using 1-hexanol and carbon dioxide as a reference system. The results were compared with corresponding literature data [54]. Details are given in section S2b of the Supporting Information.

2.4 Interfacial tension – Pendant-drop method. For the investigation of the interfacial tension σ of LOHCs with dissolved H_2 in corresponding pressurized atmosphere up to p = 9 MPa and T = 523 K, another new apparatus has been established. The used principle of pendant-drop tensiometry relies on the theoretical description of the profiles of axisymmetric drops exposed to gravity by application of the Young-Laplace equation [55–57]. A schematic representation of the apparatus is depicted in Figure 2. In this setup, pendant drops are formed at the tip of a stainless-steel capillary located inside a sample cell made of H_2-resistant stainless steel with an inner volume of about 45 mL. The cell provides optical access to the capillary and the pendant drop by

four windows. As the capillary is used as calibration reference, the exact diameter at its tip was determined using a micrometer screw with an absolute uncertainty (k = 2) of 0.01 mm. In experiments reported here, two capillaries with outer diameters of (1.575 and 1.595) mm and an inner diameter of 0.12 mm were used.

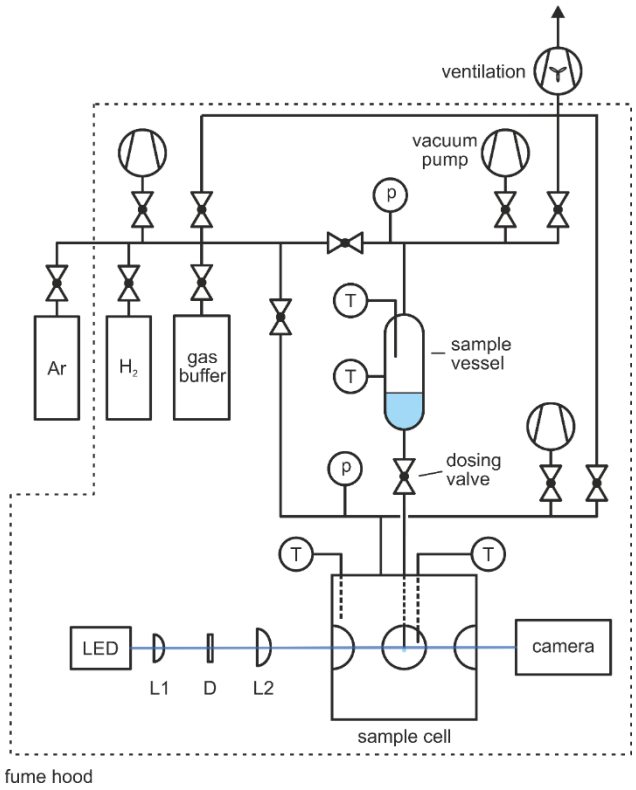

Figure 2 - Schematic representation of the new experimental setup for determination of interfacial tension of LOHCs in pressurized H_2 atmosphere by the pendant-drop method. For measurements at p = 0.1 MPa, the sample vessel is substituted by a glass syringe. (designed for single column, color only in online publication)

The T control of the sample cell is realized by resistance heating based on T measured in the cell body close to its outer wall. Additional resistance heating is placed around the optical accesses to prevent condensation at the windows. To measure the reported T in the vicinity of the pendant drops, a T probe is immersed into the gas atmosphere inside the sample cell. Here, T

stabilities better than ±0.03 K at $T \leq 448$ K, ±0.05 K for T = (473 to 498) K, and ±0.10 K at T = 523 K were achieved in measurements with Ar atmosphere at $p \approx 0.1$ MPa. The T stabilities in measurements with H_2 were better than ±0.04 K at $T \leq 423$ K and ±0.08 K for T = (498 and 523) K.

For evacuating, flushing, and pressurizing with gas, the sample cell is connected to a manifold system. p inside the sample cell is measured with a calibrated pressure transducer with an expanded uncertainty (k = 2) of 5 kPa. The p stability in the sample cell during measurements in pressurized H_2 atmosphere was better than ±(2, 21, 40, 60, and 89) kPa at $p \approx$ (0.1, 1.5, 3.0, 5.0, and 7.0) MPa, respectively. For measurements at p = 0.1 MPa, the liquid sample was contained in a gas-tight glass syringe with a volume of 5 mL, which was directly connected to a dosing valve through which the liquid was supplied to the capillary. For measurements in pressurized gas atmosphere, the liquid of investigation was contained in a separate T-controlled H_2-resistant stainless-steel vessel with an inner volume of 150 mL, which was connected to the dosing valve in place of the syringe. The vessel allows for preconditioning of the liquid close to the measurement conditions inside the sample cell. A T probe is immersed into the vessel to measure T of the gas atmosphere above the liquid level of the sample, which was adjusted within a range of ±5 K around T measured in the sample cell. The vessel can be evacuated, flushed, and pressurized with the gas of interest for presaturation of the liquid sample. p inside the vessel is measured by another calibrated pressure transducer of the mentioned type. All T measurements were performed with Pt100 resistance probes calibrated to an absolute uncertainty (k = 2) of 0.02 K.

The apparatus features a monochromatic CMOS camera with a resolution of 1936 x 1216 pixels for image acquisition, which is equipped with a 10x manual zoom lens as well as a linear

translational stage for fine adjustment of the camera position. As background illumination, a monochromatic LED with a nominal wavelength of 470 nm is used to minimize chromatic aberration effects. Plano-convex lenses (L) are used to focus the light onto a ground glass diffuser (D) and for its subsequent collimation to optimize the image sharpness.

All LOHC samples were investigated in Ar atmosphere at p = 0.1 MPa in the T range from (303 to 523) K and in H_2 atmosphere at T = (323, 423, and 498 or 523) K within a p range from (0.1 to 7) MPa. After cleaning of all components contacting the liquid sample, about (1 or 8) mL of the sample were filled into the syringe or the sample vessel, respectively. Then, the setup was flushed with Ar several times to generate an Ar atmosphere. After each T increase within a measurement series aiming at σ data in Ar atmosphere, p in the closed sample cell was reduced to p = 0.1 MPa by releasing the excess Ar to the ambience. At the beginning of each measurement series studying the influence of H_2, a measurement in Ar atmosphere at T = 323 K and p = 0.1 MPa was performed to obtain a reference value for the identical liquid sample. Then, the sample cell was evacuated and H_2 was injected. Here, p in the sample vessel was always set between (0.006 and 0.212) MPa higher than in the sample cell to ensure liquid flow through the capillary. The generation of pendant drops was started after T inside the sample cell volume had stabilized for more than 10 min each time T was varied in measurements with Ar atmosphere, and after more than 20 min each time T or p were varied in measurement series with H_2. At least 4 pendant drops with a volume of about 10 µL were generated for each investigated thermodynamic state, where the time given for droplets to equilibrate prior to starting the acquisition of images was at least 5 min at $T \leq 448$ K and at least 2 min for $T \geq 473$ K. For each drop, several images were saved in time intervals of (15 to 30) s. As rapid shrinking of produced drops could be observed in measurements at $p \approx 0.1$ MPa and T = 523 K due to the vicinity to the

boiling points of the investigated substances, images were immediately acquired without equilibration time in this case. Here, only one image was recorded for each of the at least 9 drops generated to achieve adequate measurement statistics. During the time span in which images were saved for each droplet, T and p inside the sample cell were continuously recorded and averaged for the following evaluation.

The image analysis is realized by custom-made evaluation software using the method of axisymmetric drop shape analysis (ADSA) [58–60]. Here, σ of the investigated fluid is determined by finding the theoretically calculated drop profile that fits best with the experimentally obtained drop shape. Calibration of the images was performed for conversion of the length scale from pixels to metric dimensions by using the outer diameter of the capillary. For the first image of each investigated droplet, the edges of the capillary tip were identified by a Canny edge detection algorithm [61]. The horizontal distances of the edge pixels were averaged over a vertical range of 50 pixels to yield the diameter of the capillary. The corresponding values obtained for all droplets investigated at the same thermodynamic state were averaged for the calculation of the calibration factor using the metric capillary diameter. For the analysis of images of pendant drops, the droplet edge pixels are identified by analyzing the horizontal and vertical changes in the measured gray values. In a next step, the Young-Laplace equation [55]

$$\frac{\partial \varphi}{\partial s} = \frac{2}{R} - \frac{\left(\rho_{\text{liquid}} - \rho_{\text{gas}}\right) g z}{\sigma} - \frac{\sin \varphi}{x} \tag{1}$$

is solved to calculate theoretical drop profiles. The geometrical quantities included in Eq. 1 are illustrated in Figure 3, where φ is the angle between the horizontal axis and the tangent on a

point P, *s* is the arc length along the drop contour from the apex point O to point P, and *R* represents the radius of a circle whose curvature matches that of the droplet at its apex.

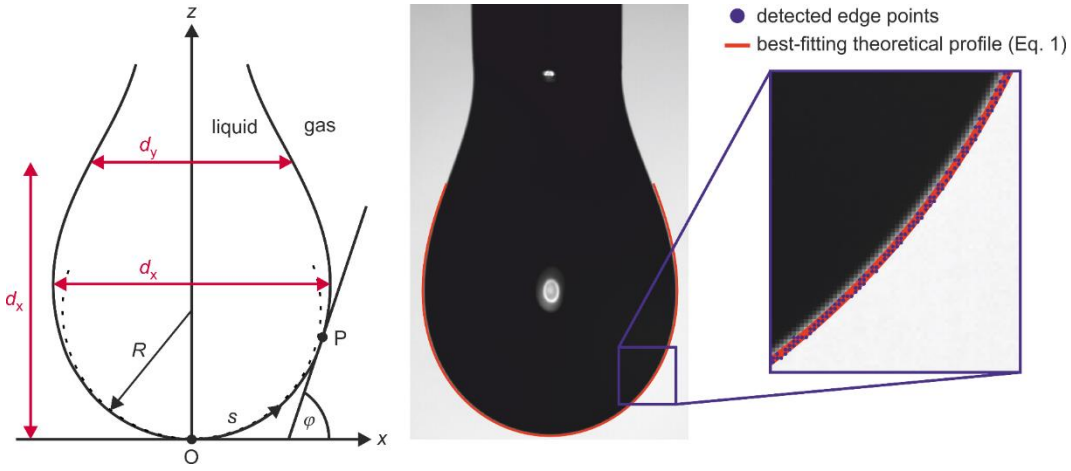

Figure 3 - Geometrical quantities for the theoretical description of pendant-drop shapes by the Young-Laplace equation and the Bond number (left part), droplet image with best-fitting theoretical profile found by the evaluation software (red line) (middle part), and a magnification of the droplet edge showing the detected edge pixels (blue dots) and the best-fitting profile (red line) (right part). (designed for 1.5 column, color only in online publication)

Before the calculation of suitable theoretical drop profiles by numerical solution of the Young-Laplace equation using a 4th-order Runge-Kutta algorithm [62,63], appropriate starting values for σ and *R* are determined. For *R*, the starting value was calculated by applying a circle-fit function [64] to the apex of the experimentally detected drop shape. Using the determined *R* together with an approximation for the Bond number or shape factor proposed by Hansen et al. [65], a starting value for σ was determined. The approximation incorporates the characteristics of the experimental profile, which are the maximum droplet width d_x as well as the droplet width d_y at the vertical coordinate with distance d_x from the apex as shown in Figure 3. The horizontal coordinate of the apex was determined by finding the middle of the lowest pixel line. Further

quantities required for the calculation are the gravitational acceleration, g = 9.81 m·s^{-2}, as well as the densities of the liquid and the gas phase. A first set of theoretical drop profiles was calculated including independent variation of R and σ within a range of about ±10% around their starting values in 40 steps. The theoretical profile with the minimum deviation from the experimental shape, considering the edge pixels from the apex (z = 0) to the vertical coordinate $z = d_x$, provides intermediate values of R and σ. Around these values, a finer independent variation within ±1% in 40 steps is performed to determine the final values by comparison of the theoretical drop profiles with the experimental one. This procedure is repeated for several apex positions to account for possible errors in its detection. Here, the detected apex position is shifted by ±(0.5 and 1) pixels in horizontal and vertical direction in steps of (0.2 and 0.4) pixels, respectively. From the best-fitting combination of theoretical and experimental drop profile, σ is taken for further processing. The reported σ data were obtained by averaging the results for all individual images recorded for a given thermodynamic state.

The required liquid density ρ' of the LOHC substances investigated in Ar atmosphere at p = 0.1 MPa was calculated from the correlations based on Eq. 2 employing the fit parameters listed in Table 2, cf. section 3.1. For measurements with pressurized H_2, ρ' was determined according to the procedure described in section S1c of the Supporting Information based on the ρ' measurements close to saturation with H_2. As ρ' was not measured in presence of H_2 for the binary mixture, its ρ' was calculated from Eq. 2 at the corresponding T for the evaluation of σ measured with dissolved H_2. This can be justified by the observation that for all other LOHC samples, the deviation of the ρ' data measured close to saturation with H_2 in the complete p range from the values obtained at p = 0.1 MPa was within the uncertainties considering also the inter-

and extrapolation procedures, cf. sections 3.1 and S1c. For determining the densities ρ'' of the gas phase, its saturation with the investigated liquid close to the pendant drop was assumed. The contribution of the LOHC vapor is estimated via the vapor pressure of the LOHC samples determined as described in section 2.3. After subtracting the vapor pressure of the LOHC sample from the measured p, the contribution of the gas added to the atmosphere was calculated from EoS for Ar [66] and H_2 [49] implemented in REFPROP [37]. Considering all assumptions made for calculating ρ'' by adding up both contributions, its expanded relative uncertainty (k = 2) is estimated to be 10%.

To evaluate the uncertainty of σ data obtained with the described experimental and evaluation procedures, results from measurements with *n*-dodecane, ethylene glycol, water, and 1,1,1,2,2,3,4,5,5,5-decafluoro-3-methoxy-4-(trifluoromethyl)-pentane (HFE-7300) were compared with reference data [67–70]. Detailed information on the reference measurements as well as the estimation of the resulting uncertainties is given in section S3 of the Supporting Information. It shows that the expanded relative uncertainty (k = 2) of the reported σ data can be estimated to $U_r(\sigma)$ = 2%, which also includes a relative uncertainty of ρ' up to $U_r(\rho')$ = 0.3%. If ρ' data with larger uncertainty are used, the value by which $U_r(\rho')$ exceeds 0.3% is added to $U_r(\sigma)$ = 2% owing to the direct influence of ρ' on the resulting σ data. For measurements at T = 523 K and $p \approx 0.1$ MPa reported here, the additional impact of droplet shrinking is assumed to be considered by an increased expanded uncertainty of $U_r(\sigma)$ = 3%.

3. Results and Discussion

3.1 Density. For both investigated mixtures, the liquid densities ρ' measured at p = 0.1 MPa are summarized in Table S1 of the Supporting Information. For the preparation of the binary mixture

investigated here, the H12-DPM sample A was used. A functional relationship between ρ' and the temperature T was established by correlation with a second-order polynomial,

$$\rho'_{\mathrm{calc}}(T) = \rho'_0 + \rho'_1 T + \rho'_2 T^2 , \tag{2}$$

where each data point was given the same statistical weight. In Table 2, the fit coefficients ρ'_0, ρ'_1, and ρ'_2 as well as the standard percentage deviation (rms) of the fit from the experimental ρ' data are summarized for both mixtures together with the corresponding information reported for H0-DPM and H12-DPM (sample A) in our previous study [35].

Due to the good quality of the fits, the experimental uncertainties of the ρ' measurements given in Table S1 can also be assigned to densities calculated using Eq. 2 for $T \leq 473.15$ K. Densities calculated at higher T required for the evaluation of pendant-drop measurements represent an extrapolation of the fit. Their uncertainties were estimated by calculating the deviations of Eq. 2 from unweighted fits of the experimental ρ' data using first- and third-order polynomials. Hence, the estimated expanded relative uncertainty (k = 2) of extrapolated ρ'_{calc} within the T range from (498 to 523) K is (0.3 and 0.2)% for the reaction and the binary mixture, respectively. For ρ'_{calc} of H0-DPM and H12-DPM, the corresponding uncertainties of extrapolated values are taken from ref. [35].

Table 2 - Coefficients of Eq. 2 for calculation of the liquid density $\rho'_{\mathrm{calc}}(T)$ of the substances studied at p = 0.1 MPa. Both mixtures had a DoH of 0.551.

Sample	ρ'_0 / (kg·m^{-3})	ρ'_1 / (kg·m^{-3}·K^{-1})	ρ'_2 / (kg·m^{-3}·K^{-2})	rms[a]
H0-DPM[b]	1228.59	–0.742262	-6.47486×10^{-5}	0.011
H12-DPM (A)[b]	1078.82	–0.679731	-4.11397×10^{-5}	0.018
Reaction mixture	1133.53	–0.691450	-6.16146×10^{-5}	0.009
Binary mixture[c]	1135.38	–0.703435	-5.07678×10^{-5}	0.009

[a]Standard percentage deviation of measured ρ' data to the fit. [b]Data from ref. [35]. [c]The mixture contained H12-DPM sample A.

Comparing the measured ρ' data of both mixtures, ρ' of the reaction mixture was on average 0.10% higher than ρ' of the binary mixture up to T = 363 K for values measured with the DMA 5000 M, and on average 0.14% higher from (373 to 473) K measured with the DMA 4200 M. Similar deviations can be found in ρ' data of mixtures of the H0-DBT/H18-DBT system reported by Müller et al. [22]. For this system, ρ' of isomeric mixtures containing only the partially hydrogenated H6-DBT or H12-DBT as well as of several reaction mixtures with different DoH showed an average relative deviation of 0.2% from binary mixtures of H0-DBT and H18-DBT with the same DoH. For the H0-DPM/H12-DPM LOHC system, no ρ' data of mixtures could be found in the literature.

The measured densities of the compressed liquid phase of H0-DPM, H12-DPM (sample C), and the reaction mixture in absence of H_2 are listed in Table 3 and illustrated in Figure 4 as a function of p, where the lines represent unweighted linear fits at given T of the data series including the corresponding ρ' data measured at p = 0.1 MPa. Since the H12-DPM sample C exhibits nearly the same purity as sample A, which was used for ρ' measurements at p = 0.1 MPa, it is assumed that combination of the data is possible without the need of considering increased uncertainties. In general, ρ' of the H_2-free samples increases with increasing p at constant T. The relative increase at a given T is similar for H12-DPM and the reaction mixture, whereas it tends to be slightly smaller for H0-DPM.

Literature data for the compressed liquid phase density of the substances studied here in absence of H_2 could only be found for H0-DPM, which were experimentally determined by Chang et al. [42]. For the only matching T of their and our study of 373 K, Figure 4 shows the agreement within the uncertainties of ρ' data from the present work.

Table 3 - Compressed liquid phase density ρ' of H0-DPM, H12-DPM (sample C), and the reaction mixture with a DoH of 0.551 in absence of H_2, measured as a function of total pressure p and temperature T.[a]

T / K	p / MPa	ρ' / (kg·m^{-3})	p / MPa	ρ' / (kg·m^{-3})	p / MPa	ρ' / (kg·m^{-3})
	H0-DPM		**H12-DPM**		**Reaction mixture**	
298.15	3.009	1003.56	3.006	874.03	3.001	923.91
	6.977	1005.64	7.000	876.33	7.006	926.17
	9.981	1007.20	10.001	878.03	9.982	927.84
323.15	3.004	984.05	1.007	855.15	3.000	905.79
	7.000	986.40	2.013	855.83	6.998	908.32
	9.968	988.11	3.008	856.49	10.002	910.18
			6.999	859.08		
			10.001	860.98		
348.15	3.002	964.60	2.997	839.02	2.995	887.69
	6.997	967.25	7.000	841.99	6.991	890.57
	9.995	969.19	9.994	844.12	9.994	892.66
373.15	3.002	945.09	3.007	821.56	3.002	869.52
	6.997	948.08	7.002	824.90	6.986	872.76
	9.995	950.26	10.030	827.36	10.004	875.19
398.15	3.001	925.52	3.004	804.09	3.005	851.31
	6.993	928.89	7.103	808.09	7.001	854.99
	9.993	931.36	9.989	810.58	10.004	857.65
423.15	3.008	905.66	3.004	786.34	3.006	832.78
	6.990	909.47	6.999	790.66	7.008	836.96
	9.998	912.25	9.999	793.73	10.009	839.96
448.15	3.003	885.46	3.000	768.28	3.000	813.91
	7.001	889.82	7.001	773.26	7.041	818.73
	9.990	893.26	9.995	776.76	10.007	822.10
473.15	3.002	864.83	3.003	749.88	3.003	794.60
	6.990	869.82	7.005	755.60	6.997	800.09
	9.998	873.41	10.000	759.59	10.013	803.99

[a]The uncertainties are $U(p)$ = 0.015 MPa as well as $U(T)$ = 0.03 K, while the relative expanded uncertainty of ρ' is $U_r(\rho')$ = 0.1%. All uncertainties are given on a confidence level of 0.95.

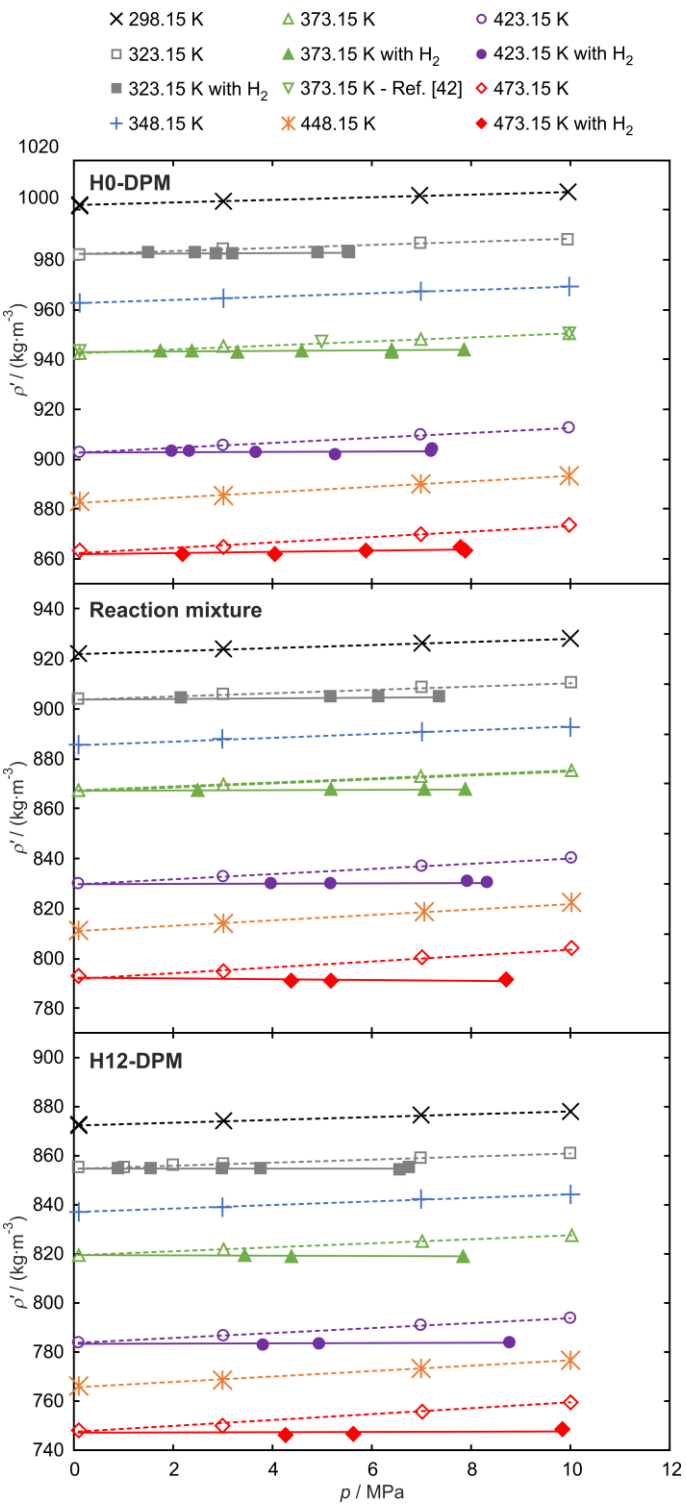

Figure 4 - Compressed liquid phase density in absence of H_2 (open symbols, linear unweighted fit represented as dashed line) as well as liquid density close to saturation with H_2 (solid symbols, linear unweighted fit represented as solid line) of H0-DPM (top part), H12-DPM

(sample C) (bottom part), and the reaction mixture with DoH = 0.551 (middle part) as a function of *p*. For H0-DPM, literature data for the compressed liquid phase density in absence of H_2 from Chang et al. [42] are shown at *T* = 373.15 K (open triangles pointing downward). (designed for single column, color only in online publication)

Figure 4 also shows the density data for the liquid phase close to saturation with H_2. The corresponding experimental values are given in Table 4 together with their uncertainties and mole fractions of H_2 dissolved in the liquid phase. The latter are the experimental values from the associated solubility measurements, but are referred to as *x* here as density was measured at slightly different *T*. To ensure comparability in Figure 4, the experimental ρ' data with dissolved H_2 were slightly shifted to the values related to the *T* values applied in the measurements without H_2 according to the procedure described in section S1c of the Supporting Information. The ρ' data with dissolved H_2 are significantly smaller than those without H_2 at the same *T* and *p*, and they hardly depend on *p* for a given *T*. The increasing deviation from the data without H_2 with increasing *p* can be attributed to the increasing H_2 solubility. This may be explained by weakened interactions between LOHC molecules in the presence of dissolved H_2.

Table 4 - Liquid density ρ' of H0-DPM, H12-DPM (sample C), and the reaction mixture with DoH = 0.551 close to saturation with H_2 as a function of temperature *T* and pressure *p* as well as the corresponding mole fractions *x* of H_2 in the liquid phase measured in the VLE cell by the isochoric-saturation method given in Table 5.[a]

T / K	p^b / MPa	100·*x*	ρ' / (kg·m^{-3})	*T* / K	p^b / MPa	100·*x*	ρ' / (kg·m^{-3})
H0-DPM							
324.15	1.498	0.49	981.89		7.873	4.14	943.46
	2.447	0.83	981.90	425.35	1.973	1.31	901.27

	5.526	1.79	982.36		2.337	1.55	901.35
373.85	1.741	0.85	942.64		7.227	4.69	902.29
	2.379	1.17	942.69	470.65	2.184	1.75	863.75
	6.412	3.11	943.19		7.883	6.25	865.36
H12-DPM (C)							
323.15	0.895	0.28	854.54		7.823	5.82	819.03
	1.539	0.59	854.59	423.15	3.812	3.39	782.93
	2.985	1.30	854.56		4.942	4.56	783.24
	3.754	2.18	854.64		8.768	7.75	783.78
	6.756	3.74	855.03	473.15	4.241	4.54	745.89
	6.548	4.31	854.07		5.605	5.93	746.58
373.15	3.423	2.33	819.24		9.813	10.14	748.46
	4.363	3.39	818.93				
Reaction mixture							
324.15	2.157	0.99	903.39	423.65	3.963	3.41	829.31
	5.169	2.61	903.76		5.171	4.62	829.48
	6.125	3.03	903.79		7.930	7.10	830.15
	7.360	3.90	904.03		8.311	7.61	829.61
373.85	2.493	1.62	866.75	470.65	4.375	4.75	792.60
	5.172	3.58	867.01		5.158	5.65	792.68
	7.050	4.89	867.07		8.683	9.36	793.36
	7.880	5.70	867.36				

[a]The uncertainties are $U(p)$ = 0.015 MPa as well as $U(T)$ = 0.03 K. As x is equal to x_s measured in the VLE cell in solubility measurements, the uncertainty of x corresponds to the uncertainties of x_s listed in Table 5 at the state points close to the state points reported in the present table. The expanded relative uncertainty of ρ' is $U_r(\rho')$ = 0.2%. All uncertainties are given on a confidence level of 0.95.
[b]p is the average of the values measured with the transducers in the VLE cell and the circulation loop. In any case, the deviation from the mean value is smaller than $U(p)$.

3.2 Solubility. The H_2 solubility in H0-DPM and H12-DPM (sample C) was measured to determine its difference related to the pure non-hydrogenated and fully hydrogenated compounds. In addition, a reaction mixture with a DoH of 0.551 obtained from a deliberately

stopped hydrogenation experiment was studied to evaluate to which extent knowledge on the H_2 solubility in H0-DPM and H12-DPM is transferable to mixtures being present in realistic technical processes. The measured H_2 solubility in the LOHCs expressed in form of the mole fraction x_s of H_2 dissolved in the liquid phase as well as the corresponding expanded absolute uncertainties ($k = 2$) $U(x_s)$ are given in Table 5. The given ρ' data used as input for the evaluation of the solubility were obtained by adjusting measured densities at similar T to that in the VLE cell by the procedure explained in section S1c of the Supporting Information. A representation of p as a function of x_s at different T, which represent the average of all similar T in the corresponding measurement series, is shown in Figure 5 for all studied substances.

Table 5 - Experimental H_2 solubility expressed as mole fraction x_s of H_2 dissolved in H0-DPM, H12-DPM (sample C), and the reaction mixture with DoH = 0.551 as a function of temperature T and pressure p.[a]

Sample	T / K	p^b / MPa	ρ' / (kg·m^{-3})	100·x_s	100·$U(x_s)$
H0-DPM	323.64 ± 0.02	1.498	982.3	0.49	0.15
	323.60 ± 0.02	2.447	982.3	0.83	0.25
	323.58 ± 0.02	5.526	982.8	1.79	0.29
	374.09 ± 0.21	1.741	942.4	0.85	0.14
	374.12 ± 0.22	2.379	942.5	1.17	0.22
	374.29 ± 0.22	6.412	942.8	3.11	0.29
	374.21 ± 0.20	7.873	943.2	4.14	0.32
	425.26 ± 0.76	1.973	901.3	1.31	0.14
	424.63 ± 0.77	2.337	901.9	1.55	0.18
	424.51 ± 0.75	7.227	903.0	4.69	0.29
	469.87 ± 1.26	2.184	864.4	1.75	0.13
	469.89 ± 1.27	7.883	866.0	6.25	0.28
H12-DPM (C)	323.98 ± 0.10	0.895	853.9	0.28	0.14

	323.92 ± 0.05	1.539	854.0	0.59	0.19
	323.93 ± 0.06	2.985	854.0	1.30	0.23
	325.03 ± 0.08	3.754	853.3	2.18	0.26
	323.84 ± 0.05	6.756	854.5	3.74	0.31
	324.94 ± 0.09	6.548	852.8	4.31	0.30
	374.92 ± 0.41	3.423	818.0	2.33	0.22
	377.40 ± 0.10	4.363	815.9	3.39	0.25
	377.28 ± 0.13	7.823	816.1	5.82	0.30
	425.63 ± 0.56	3.812	781.2	3.39	0.22
	425.74 ± 0.52	4.942	781.4	4.56	0.25
	425.76 ± 0.43	8.768	781.9	7.75	0.29
	476.66 ± 0.69	4.241	743.4	4.54	0.21
	476.64 ± 0.67	5.605	744.1	5.93	0.25
	480.86 ± 0.49	9.813	743.0	10.14	0.28
Reaction mixture	323.69 ± 0.10	2.157	903.7	0.99	0.17
	323.22 ± 0.02	5.169	904.5	2.61	0.32
	323.10 ± 0.02	6.125	904.6	3.03	0.34
	323.12 ± 0.02	7.360	904.8	3.90	0.40
	373.49 ± 0.16	2.493	867.0	1.62	0.16
	373.38 ± 0.24	5.172	867.4	3.58	0.29
	373.11 ± 0.24	7.050	867.6	4.89	0.34
	373.07 ± 0.26	7.880	868.0	5.70	0.38
	423.84 ± 0.84	3.963	829.2	3.41	0.20
	423.84 ± 0.87	5.171	829.3	4.62	0.26
	423.21 ± 0.79	7.930	830.5	7.10	0.33
	423.08 ± 0.82	8.311	830.0	7.61	0.36
	471.50 ± 1.40	4.375	792.0	4.75	0.20
	471.68 ± 1.35	5.158	791.9	5.65	0.23
	468.47 ± 1.34	8.683	795.0	9.36	0.33

[a]The uncertainty $U(p)$ is 0.015 MPa. The uncertainty $U(T)$ is given in the table. It considers the uncertainty of the calibrated T probes of 0.02 K. If this value is exceeded by the difference between the mean values obtained with the individual T probes close to the gas and liquid phase and their average value, the reported uncertainties $U(T)$ are expressed by this difference. The relative uncertainty $U_r(\rho')$ estimated according to section S1c is 0.2%. The absolute uncertainties

$U(x_s)$ are calculated by error propagation in quadrature and are given in the table. All uncertainties are specified on a confidence level of 0.95.
[b]p is the averaged pressure measured with the transducers in the VLE cell and the circulation loop. The deviation of the individual pressures from the reported mean values are smaller than $U(p)$.

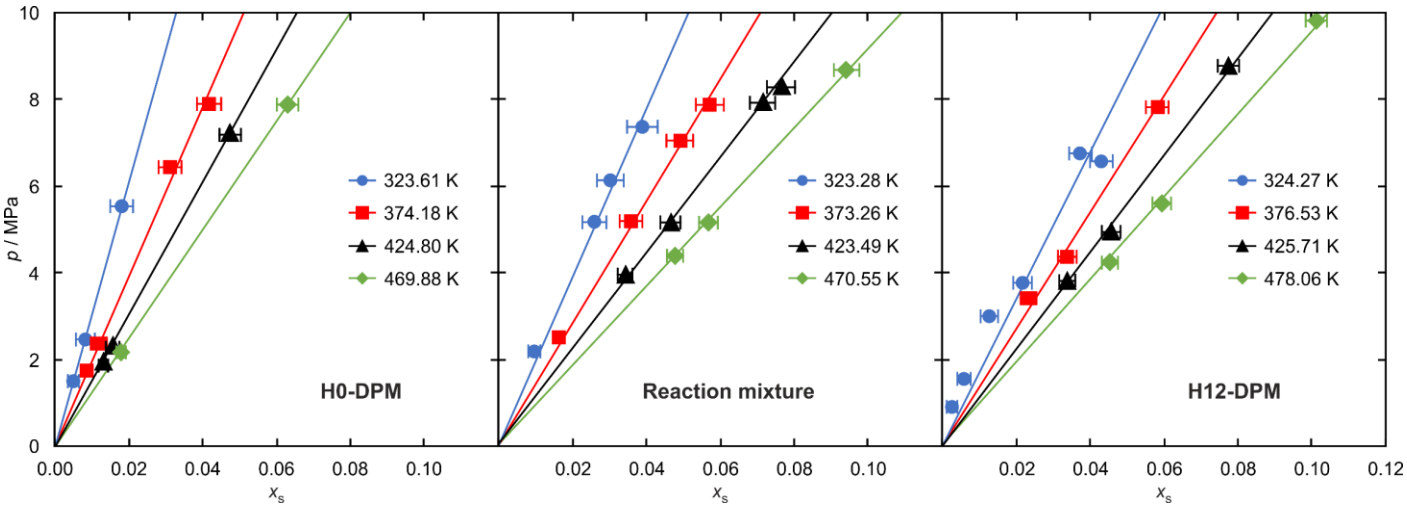

Figure 5 - Total pressure p at VLE of H_2 with H0-DPM (left), the reaction mixture with DoH = 0.551 (middle), and H12-DPM (sample C) (right), as a function of the mole fraction of dissolved H_2 x_s at different averaged temperatures T. The lines represent linear fits of the data as a function of x_s intercepting the vertical axis at the vapor pressures of the LOHC samples. (designed for double column, color only in online publication)

x_s shows linear p-dependent trends within the investigated p range for all T and substances. Therefore, the corresponding slope in form of the constant H is determined for each T by approximating Henry´s law using the relation

$$p = Hx_s + p_{vap}, \tag{3}$$

where p_{vap} is the vapor pressure of the solvent at the averaged T. The data at given T are fitted linearly in the full p range studied with constraining x_s = 0 to the vapor pressures of the LOHC samples. Apart from the series at T = 323 K for H12-DPM, all measured values match within uncertainties with the linear fits. For this exceptional case, equilibrium of the system had

probably not been reached for the three smallest p due to a too low pumping speed at the beginning of the measurement series. The results for H are summarized in Table 6 for each substance and T and are shown as a function of T in Figure 6. The worst-case limits associated with each H value were determined by repeating the linear fitting after varying $x_s \pm U(x_s)$ for each data point.

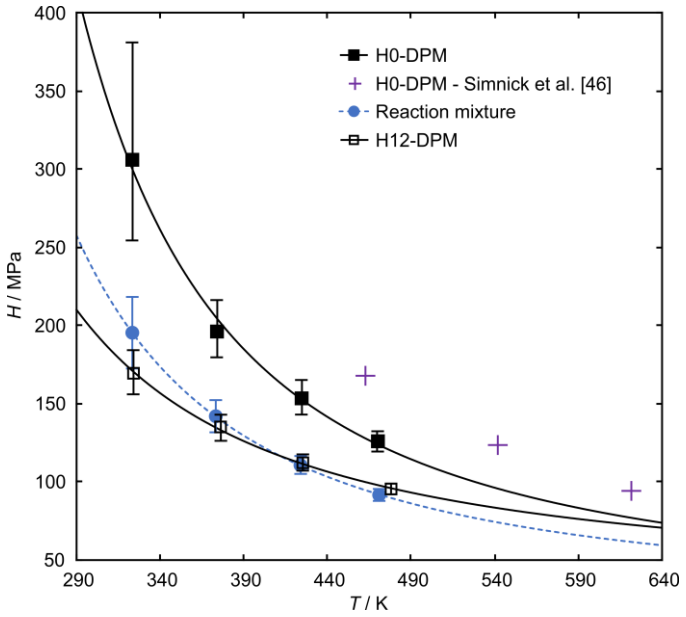

Figure 6 - Constants H of Eq. 3 for H0-DPM, H12-DPM (sample C), and the reaction mixture with a DoH of 0.551 as a function of T. The lines represent the fits of the corresponding systems by Eq. 4 with the coefficients given in Table 6. (designed for single column, colors only in online publication)

Table 6 – Determined constants H of Eq. 3 with their upper and lower worst-case limits $U(H)^+$ and $U(H)^-$ for H0-DPM, H12-DPM (sample C), and the reaction mixture with a DoH of 0.551 as a function of temperature T.[a]

Sample	T / K	H / MPa	$U(H)^+$ / MPa	$U(H)^-$ / MPa
H0-DPM	323.61 ± 0.03	306.3	378.5	255.8
	374.18 ± 0.11	196.4	215.4	180.3

	424.80 ± 0.46	153.6	164.8	143.6
	469.88 ± 0.01	125.7	132.0	120.0
H12-DPM (C)	324.27 ± 0.76	169.3	184.4	156.0
	376.53 ± 1.61	134.5	143.2	126.7
	425.71 ± 0.08	111.8	117.1	107.0
	478.06 ± 2.81	95.3	98.6	92.2
Reaction mixture	323.28 ± 0.41	195.5	220.0	175.9
	373.26 ± 0.23	141.9	152.6	132.5
	423.49 ± 0.41	111.0	116.8	105.8
	470.55 ± 2.08	92.0	95.7	88.6

[a]The reported T values are the averages of the individual values given in Table 5. The given T intervals represent the maximum differences between the individual T values and their average. $U(H)^+$ and $U(H)^-$ represent the estimated worst-case limits of H.

The H values obtained for each substance were correlated by

$$\ln\left[H(T)/\mathrm{MPa}\right] = H_0 + H_1 \cdot (\mathrm{K}/T) \tag{4}$$

as proposed by Hefter and Tomkins [71] with a power series with truncation after the second term. The fit coefficients H_0 and H_1 and the quality of the fit, expressed by the average absolute relative deviation (AARD) of the individual H data from the fit, are summarized in Table 7. By using $H(T)$ obtained from Eq. 4, the H_2 solubility $x_{s,calc}(T,p)$ can be calculated from Eq. 3, as realized in the present study to determine x_s for the state points investigated by the pendant-drop method.

Table 7 - Coefficients of Eq. 4 for the calculation of $H(T)$ for the LOHC systems studied.

Sample	H_0	H_1	AARD / %[a]
H0-DPM	2.87	917	1.97
H12-DPM (C)	3.35	579	0.71
Reaction mixture	2.87	778	0.15

[a]Average absolute relative deviation (AARD) of $H(T)$ reported in Table 6 from the fit.

The solubility of H_2 at a given p and T is about 50% higher in the fully hydrogenated H12-DPM than in the dehydrogenated H0-DPM, which agrees with findings for the behavior of H_2 solubility in other LOHC systems, *i.e.*, H0-DBT/H18-DBT, H0-NEC/H12-NEC, toluene/methylcyclohexane, and benzene/cyclohexane [14,16]. Furthermore, the reaction mixture, which mainly consists of H6-DPM, exhibits similar H_2 solubility as the fully hydrogenated H12-DPM. Considering the associated uncertainties of $H(T)$ for H12-DPM and the reaction mixture, no significant difference is found. This might be partially related to the smaller mole fraction $x_{\text{H0-DPM}} = 0.098$ compared to $x_{\text{H12-DPM}} = 0.200$ in the reaction mixture. However, a more detailed analysis on intermolecular interactions in the mixtures would be necessary to find the exact reasons for the observed behavior. Literature data for H_2 solubility in mixtures of the compounds of specific LOHC systems that could be used for comparison are not available to the best of our knowledge.

For all systems and the T range studied here, the H_2 solubility increases with increasing T as it has been reported in the literature for H0-DPM [45,46]. Cukor and Prausnitz [45] investigated H0-DPM at $p \leq 0.1$ MPa by the isochoric-saturation method realized as described by Dymond and Hildebrand [72]. For the dilute mixtures studied, they reported Henry constants that are not directly comparable with the H values deduced from our solubility measurements at higher p. The Henry constants of Cukor and Prausnitz [45] agree with those calculated by Simnick et al. [46] from their solubility data measured for p = (2 to 25) MPa and T = (463 to 702) K. Simnick et al. [46] used a flow apparatus where after equilibration, a sample was extracted and separated into liquid and gas phase at ambient conditions in a trap. x_s was determined by measuring the volume of the desorbed H_2 and weighing the residual liquid phase.

To allow comparison with our H data, the experimental solubilities reported by Simnick et al. [46] at $p \leq 10$ MPa enclosing the pressures investigated in the present study were fitted employing Eq. 3. The resulting H values displayed in Figure 6 are significantly larger than our data for H0-DPM, which also holds in the process-relevant regime of $T > 473$ K where Eq. 4 applied to our H data for H0-DPM is extrapolated.

3.3 Interfacial tension. Interfacial tensions σ of the LOHC samples investigated in Ar atmosphere at $p = 0.1$ MPa are listed as a function of T in Table 8 together with the liquid- and gas-phase densities ρ' and ρ'' used as input for the evaluation. Here, sample B of H12-DPM was used as pure substance and as component of the binary mixture. ρ' data at the reported T were calculated by Eq. 2 using the corresponding fit coefficients from Table 2. Although a T-dependent ρ' correlation for the H12-DPM sample B is available from Berger Bioucas et al. [73], the fit parameters for the H12-DPM sample A from Kerscher et al. [35] were used in this work, as the latter are based on ρ' data measured up to $T = 473.15$ K. The influence of the deviation of about 0.2% between these ρ' data for the samples A and B on the determined σ is covered by the measurement uncertainties described in section 2.4. At state points where measurements were performed several times, corresponding data shown in Table 8 represent the average of the individual results. The deviation of the average σ values obtained from different images of the individual droplets from the average value for all droplets at a given state point was within the uncertainties in all cases except for H0-DPM at $T = 373.20$ K. Here, a larger negative relative deviation of about 5.1% was found for the images of an individual droplet, which was not excluded since no obvious experimental reason could be found.

Table 8 - Interfacial tension σ of H0-DPM, H12-DPM (sample B), and both mixtures with DoH ≈ 0.55 in Ar atmosphere at p = 0.1 MPa as a function of temperature T as well as liquid density ρ' from Eq. 2 and gas-phase density ρ'' calculated as described in section 2.4 and used for the data evaluation.[a]

T / K	ρ' / (kg·m^{-3})	ρ'' / (kg·m^{-3})	σ / (mN·m^{-1})	T / K	ρ' / (kg·m^{-3})	ρ'' / (kg·m^{-3})	σ / (mN·m^{-1})
H0-DPM				**H12-DPM (B)**			
303.11	997.66	1.55	38.40	303.13	868.99	1.55	31.93
323.15	981.97	1.46	36.30	323.13	854.88	1.47	29.69
348.16	962.32	1.36	33.40	348.07	837.24	1.36	27.65
373.20	942.57	1.28	30.56	373.11	819.48	1.29	25.44
398.18	922.77	1.24	29.06	398.15	801.66	1.26	23.22
423.17	902.89	1.24	25.75	423.06	783.89	1.34	21.11
448.34	882.79	1.37	24.31	448.19	765.91	1.60	19.22
473.35	862.74	1.64	21.93	473.16	747.99	2.10	17.18
498.35	842.61	2.18	19.60	498.09	730.04	2.92	15.35
523.27	822.46	3.07	17.58	523.00	712.07	4.12	13.88
Reaction mixture, DoH = 0.551				**Binary mixture, DoH = 0.545**[b]			
303.09	918.30	1.55	32.25	303.11	917.50	1.55	32.91
323.17	903.59	1.51	31.57	323.14	902.77	1.48	30.51
348.14	885.35	1.36	29.56	348.05	884.40	1.36	28.30
373.16	866.94	1.29	26.89	373.15	865.82	1.29	26.93
398.26	848.38	1.24	24.77	398.10	847.30	1.25	24.82
423.20	829.88	1.30	22.86	423.14	828.63	1.30	23.36
473.14	792.59	1.89	18.71	472.97	791.32	1.89	18.57
522.89	755.13	3.61	14.68	522.89	753.68	3.63	14.59

[a]The relative uncertainty $U_r(\sigma)$ is 2% for $T \leq 498$ K and 3% for T = 523 K. The relative uncertainties for ρ' of the mixtures are given in Table S1 of the Supporting Information for $T \leq$ 473 K, which are identical to $U_r(\rho')$ of H0-DPM and H12-DPM (sample A) reported for measurements with the different densimeters at the corresponding T [35]. The uncertainties of ρ' data extrapolated for T > 473 K are (0.3 and 0.2)% for the binary mixture and the reaction mixture, respectively, while the corresponding uncertainties for H0-DPM and H12-DPM in this T range are 0.2% [35]. The estimated relative uncertainty of the gas phase density is $U_r(\rho'')$ = 10%. The uncertainty of measured T is $U(T)$ = 0.05 K from (303 to 448) K, $U(T)$ = 0.07 K from

(473 to 498) K, and $U(T)$ = 0.12 K at 523 K, considering both the uncertainties of the used resistance probes of 0.02 K and the achieved T stabilities. All uncertainties are given on a confidence level of 0.95.
[b]The mixture contained H12-DPM sample B.

Figure 7 shows the interfacial tensions measured in Ar atmosphere, where the lines represent their unweighted linear fits as a function of T,

$$\sigma_{\mathrm{calc}}(T) = \sigma_0 + \sigma_1 \cdot T \,. \tag{5}$$

Here, σ_0 and σ_1 are the fit coefficients that are given together with the AARD of the experimental data from the fit in Table 9.

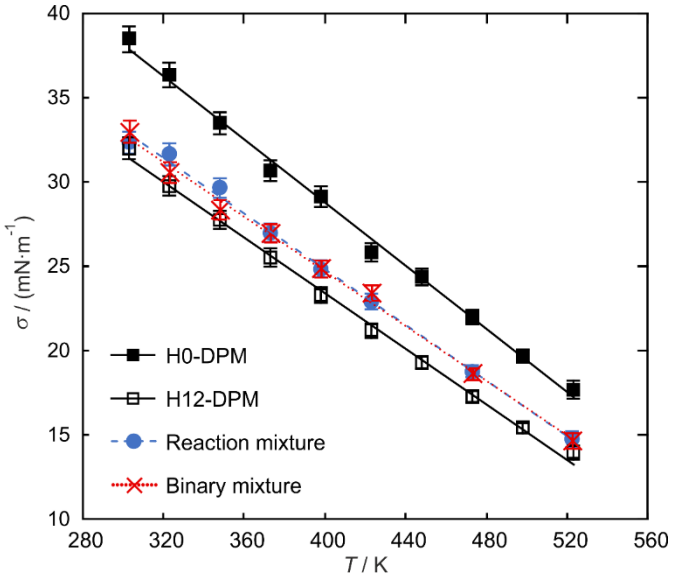

Figure 7 - Interfacial tension σ of the studied LOHCs measured in Ar atmosphere at p = 0.1 MPa (symbols) and their correlations as a function of T based on Eq. 5 (lines). (designed for single column, color only in online publication)

σ of the dehydrogenated H0-DPM is clearly larger than that of the fully hydrogenated H12-DPM. This behavior could already be found for the H0-DPM/H12-DPM system by surface light scattering (SLS) measurements in a previous study [35] and for other LOHC systems [19-

21]. It was attributed to dispersive intermolecular forces being more pronounced in the case of the unsaturated aromatic molecular structure of H0-DPM [35], which goes along with the higher liquid density of the dehydrogenated compounds. The σ data of the studied mixtures with a DoH of about 0.55 agree within their uncertainties and are between those of H0-DPM and H12-DPM. Thus, the partially hydrogenated H6-DPM species that is present at high concentration in the reaction mixture appears to have no noticeable impact on σ. As the σ data of the mixtures tend to be closer to those of H12-DPM, the latter seems to dominate the interactions at the liquid-gas interface.

Table 9 - Fit coefficients of Eq. 5 for calculation of the interfacial tension $\sigma_{calc}(T)$ of the LOHC samples studied in Ar atmosphere at p = 0.1 MPa.

Sample	σ_0 / (mN·m^{-1})	σ_1 / (mN·m^{-1}·K^{-1})	AARD[a]
H0-DPM	66.30	–0.09389	1.25%
H12-DPM (B)	56.30	–0.08230	1.25%
Reaction mixture, DoH = 0.551	57.84	–0.08260	0.80%
Binary mixture, DoH = 0.545[b]	57.02	–0.08095	1.13%

[a]Average absolute relative deviation (AARD) of experimental data points from the fit.
[b]The mixture contained H12-DPM sample B.

Figure 8 shows the relative deviation of the present experimental σ results and SLS data [35] for H0-DPM and H12-DPM from Eq. 5. In addition, the deviations of literature values from Koefoed and Villadsen [43] and Harkins and Ewing [44], which were measured by a modified capillary-rise method and the drop-weight method, respectively, are given for H0-DPM. Literature data for the mixtures are not available. To ensure legibility, error bars are presented only for some data from the present study. For H0-DPM, agreement of most of the present data points with the SLS data and the remaining literature data within combined uncertainties can be found. For H12-DPM, however, the results from the pendant-drop measurements exhibit

significantly larger values compared to those from SLS. This may be related to the different purities of the H12-DPM samples used in the pendant-drop and SLS experiments. The difference of the results could also be explained by the different experimental procedures that affect the impact of impurities. While the liquid-gas interface of the same sample is maintained and analyzed over long time intervals in SLS measurement series [35], the frequently substituted pendant drops are produced from the bulk of the liquid sample. Thus, less surface-active impurities should be able to accumulate at the surface of the pendant drops than at the interface studied by SLS.

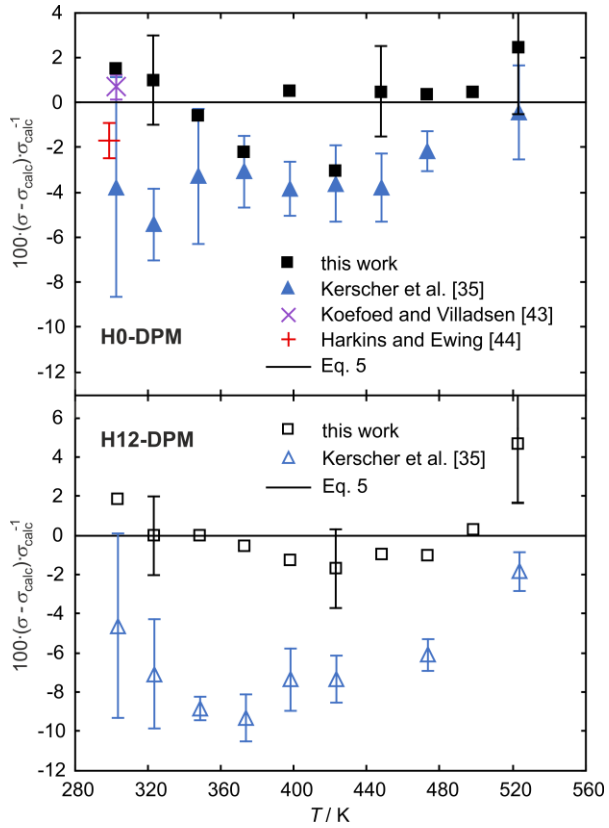

Figure 8 - Data comparison for σ of H0-DPM (upper part) and H12-DPM (lower part). The solid baselines represent the fits to the experimental data of this work based on Eq. 5. (designed for single column width, color only in online publication).

For the measurements of interfacial tension in the presence of H_2, the small droplet size, the waiting time between droplet generation and image acquisition as well as the preliminary equilibration time in the saturation vessel before the start of measurements allow the assumption that the droplets were in macroscopic thermodynamic equilibrium when the images were recorded. This is supported by the observation that σ determined from the individual images of a given droplet as well as the average σ values for the different droplets at a given state point showed no time-dependent trends. The results of the pendant-drop measurements conducted with pre-saturated LOHC in pressurized H_2 atmosphere are listed in Table 10. For studying H12-DPM with dissolved H_2, sample C was used, while sample B was contained in the binary mixture. Comparison of the σ values of sample C measured in Ar atmosphere before the injection of H_2 with the results for sample B determined in the *T*-dependent measurement series in Ar atmosphere, however, yields agreement within uncertainties. Also in the measurement series performed in the presence of H_2, the deviations of the averaged σ values from the different images of individual droplets from the average of all droplets at each state point were usually within the uncertainties. Only for H12-DPM at T = 523.09 K and p = 0.163 MPa, a minimum and maximum deviation of (4.2 and 4.9)% was found. This can be attributed to images of single droplets where the stability of the corresponding droplets was probably more affected by shrinking due to evaporation compared to all other studied droplets at this state point. Thus, an uncertainty of 3% can still be assumed for the reported average value of at least 9 single droplets before considering the impact of the uncertainty of density. The stated mole fractions x_s of H_2 in the liquid phase were obtained from Eq. 3 using *H(T)* determined from Eq. 4. To illustrate the influence of H_2 on the interfacial tension, Figure 9 depicts the relative deviations of the measured σ from the value obtained at $p \approx 0.1$ MPa in H_2 atmosphere, $\sigma_{0.1\ \mathrm{MPa}}$. For the sake of legibility,

error bars are only plotted for one T. In addition, the results of measurements performed for the identical samples in Ar atmosphere at p = 0.1 MPa and T = 323 K before the injection of H_2 are included in Figure 9. For the LOHC mixtures, they agreed with those in H_2 atmosphere close to 0.1 MPa within combined uncertainties, while the agreement is within uncertainties for H0-DPM and H12-DPM.

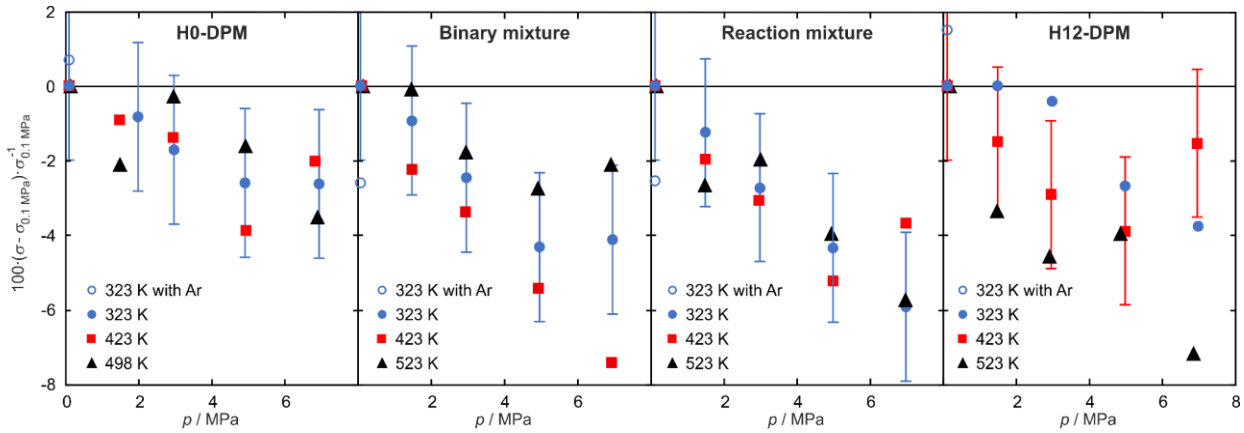

Figure 9 - Interfacial tension σ of H0-DPM, H12-DPM, the reaction mixture, and the binary mixture, both with DoH ≈ 0.55, as a function of p at different T. The results are given as relative deviations from $\sigma_{0.1\ MPa}$, which was measured at p ≈ 0.1 MPa in H_2 atmosphere at the corresponding T, and include the data for the identical samples at T = 323 K in Ar atmosphere at p = 0.1 MPa. (designed for double column, color only in online publication)

Figure 9 illustrates that σ shows a decreasing tendency with increasing p of the H_2 atmosphere and, thus, increasing x_s of dissolved H_2. Clear trends as a function of T cannot be resolved as the measured data at given p agree within their combined uncertainties. Furthermore, the p-dependent decrease in σ for a given T is similar for all LOHC samples studied although the solubility of H_2 was found to be significantly higher in H12-DPM than in H0-DPM. It seems that the p-dependent behavior is rather dominated by the presence of H_2 directly at the interface than by its integral concentration in the liquid phase.

Table 10 - Interfacial tension σ of H0-DPM, H12-DPM (C), and both mixtures with DoH ≈ 0.55 in H_2 atmosphere as a function of p and T as well as mole fractions x_s of dissolved H_2 calculated from Eq. 3, liquid density ρ' obtained from the procedure reported in section S1c of the Supporting Information, and gas phase density ρ'' calculated as described in section 2.4. The results of the measurements in Ar atmosphere of the identical sample before injection of H_2 are also listed.[a]

T / K	p / MPa	$100 \cdot x_s$	ρ' / (kg·m^{-3})	100· $U_r(\rho')$	ρ'' / (kg·m^{-3})	σ / (mN·m^{-1})	100· $U_r(\sigma)$
H0-DPM							
323.16[b]	0.099[b]	-	981.96	0.01	1.47	36.58[b]	2.0
323.44	0.111	0.04	981.8	0.3	0.08	36.32	2.0
323.45	1.996	0.66	982.0	0.3	1.48	36.03	2.0
323.44	2.995	1.00	982.1	0.3	2.21	35.70	2.0
323.44	4.931	1.64	982.3	0.3	3.64	35.38	2.0
323.46	6.957	2.32	982.5	0.3	5.02	35.37	2.0
423.34	0.116	0.07	902.2	0.3	0.24	26.49	2.0
423.34	1.482	0.96	902.2	0.3	1.02	26.25	2.0
423.25	2.950	1.91	902.3	0.3	1.84	26.13	2.0
423.35	4.949	3.22	902.3	0.3	2.95	25.46	2.0
423.25	6.836	4.44	902.5	0.3	3.97	25.96	2.0
498.16	0.128	0.08	842.4	0.6	1.66	19.89	2.3
498.33	1.482	1.30	842.4	0.6	2.32	19.47	2.3
498.40	2.946	2.62	842.5	0.6	3.02	19.83	2.3
498.44	4.919	4.40	842.9	0.6	3.95	19.57	2.3
498.41	6.896	6.18	943.1	0.6	4.87	19.19	2.3
H12-DPM (C)							
323.13[b]	0.100[b]	-	854.88	0.01	1.49	29.51[b]	2.0
323.31	0.105	0.06	854.6	0.3	0.08	29.07	2.0
323.32	1.497	0.87	854.5	0.3	1.11	29.07	2.0
323.32	2.997	1.75	854.5	0.3	2.21	28.95	2.0
323.31	4.996	2.92	854.5	0.3	3.65	28.28	2.0
323.31	6.998	4.08	854.4	0.3	5.05	27.97	2.0

423.52	0.109	0.09	783.1	0.3	0.36	21.13	2.0
423.52	1.480	1.31	783.1	0.3	1.14	20.81	2.0
423.51	2.974	2.64	783.0	0.3	1.98	20.51	2.0
423.49	4.989	4.44	783.0	0.3	3.09	20.30	2.0
423.49	6.980	6.21	783.1	0.3	4.17	20.80	2.0
523.09	0.163	0.07	710.9	0.8	4.15	13.77	3.5
523.61	1.455	1.57	710.6	0.8	4.79	13.30	2.5
523.59	2.908	3.25	710.7	0.8	5.45	13.14	2.5
523.54	4.854	5.50	710.9	0.8	6.32	13.22	2.5
523.61	6.847	7.81	711.0	0.8	7.21	12.77	2.5
Reaction mixture, DoH = 0.551							
323.24[b]	0.109[b]	-	903.59	0.01	1.62	31.25[b]	2.0
323.28	0.104	0.05	903.6	0.3	0.08	32.07	2.0
323.28	1.500	0.77	903.8	0.3	1.12	31.67	2.0
323.28	2.999	1.53	904.1	0.3	2.21	31.19	2.0
323.29	5.000	2.55	904.4	0.3	3.65	30.67	2.0
323.29	7.003	3.58	904.6	0.3	5.05	30.16	2.0
423.29	0.108	0.09	829.7	0.3	0.30	22.93	2.0
423.29	1.492	1.34	829.7	0.3	1.09	22.48	2.0
423.26	2.971	2.68	829.7	0.3	1.92	22.22	2.0
423.30	4.980	4.49	829.9	0.3	3.03	21.72	2.0
423.28	6.982	6.30	860.0	0.3	4.12	22.08	2.0
522.81	0.142	0.07	754.7	0.7	3.53	14.90	3.4
523.33	1.472	1.77	754.1	0.7	4.18	14.50	2.4
523.39	2.987	3.72	753.8	0.7	4.87	14.60	2.4
523.38	4.936	6.22	753.3	0.7	5.75	14.30	2.4
523.35	6.958	8.81	752.9	0.7	6.64	14.04	3.4
Binary mixture, DoH = 0.545[c]							
323.07[b]	0.101[b]	-	902.82	0.01	1.51	31.22[b]	2.0
323.19	0.104	-	902.73	0.3	0.08	32.06	2.0
323.21	1.508	-	902.72	0.3	1.12	31.75	2.0
323.21	3.000	-	902.72	0.3	2.21	31.27	2.0

323.21	5.005	-	902.72	0.3	3.65	30.67	2.0
323.16	6.997	-	902.76	0.3	5.05	30.73	2.0
423.01	0.109	-	828.73	0.3	0.30	23.65	2.0
423.01	1.489	-	828.70	0.3	1.09	23.11	2.0
423.06	2.973	-	828.70	0.3	1.92	22.84	2.0
423.05	4.960	-	828.70	0.3	3.02	22.36	2.0
423.07	6.967	-	828.69	0.3	4.11	21.88	2.0
522.33	0.156	-	754.10	0.7	3.52	15.07	3.4
523.01	1.467	-	753.59	0.7	4.17	15.05	2.4
523.02	2.970	-	753.58	0.7	4.86	14.80	2.4
522.93	4.948	-	753.65	0.7	5.74	14.65	2.4
523.03	6.952	-	753.58	0.7	6.64	14.75	2.4

[a] The estimated absolute uncertainty of measured T is $U(T)$ = 0.06 K at $T \leq 423$ K and $U(T)$ = 0.1 K at T = (498 and 523) K, considering the uncertainties of used resistance probes of 0.02 K and the achieved T stabilities. The reported p data have an estimated absolute uncertainty of $U(p)$ = (7, 27, 45, 66, and 94) kPa at $p \approx$ (0.1, 1.5, 3, 5, and 7) MPa, respectively, considering the uncertainties of used pressure transducers of 5 kPa and the achieved p stabilities. The relative uncertainties $U_r(\rho')$ of the liquid density, which result from the procedure reported in section S1c of the Supporting Information, are given in the table. The estimated relative uncertainty of the gas phase density is $U_r(\rho'')$ = 10%. The relative uncertainties of the measured interfacial tensions $U(\sigma)$, which also consider the uncertainty of ρ', are given in the table. All uncertainties are given on a confidence level of 0.95.

[b] Measurement performed in Ar atmosphere with the identical liquid samples before injection of H_2.

[c] The listed ρ' of the binary mixture are calculated from Eq. 2, since ρ' of the binary mixture was not measured in presence of H_2. The uncertainty of this assumption is covered by the uncertainties stated for ρ' of the other LOHC substances, which were calculated by the procedure described in section S1c of the Supporting Information. Therefore, the stated uncertainties of ρ' of the reactor mixture are also assumed for the binary mixture. The mixture contained sample B of H12-DPM.

4. Conclusions

Using two experimental setups, the H_2 solubility as well as interfacial tension and liquid density with and without dissolved H_2 were measured for the LOHC system H0-DPM/H12-DPM under process-relevant conditions. Besides the pure LOHC compounds H0-DPM and H12-DPM, a

reaction mixture with a degree of hydrogenation of 0.551 was studied to verify the influence of the reaction intermediate H6-DPM on the measured physico-chemical properties. Corresponding binary mixtures of H0-DPM and H12-DPM with the same degree of hydrogenation were additionally investigated for this purpose.

For T up to 473 K and p up to 10 MPa, the solubility of H_2 was found to be about 50% higher in the fully hydrogenated H12-DPM and in the reaction mixture compared to H0-DPM under the same conditions. Pressure-dependent measurements of the liquid density in absence of H_2 as well as close to saturation with H_2 up to 473 K and 10 MPa revealed that dissolved H_2 leads to nearly constant values for a given T and varying p. Measurements of the interfacial tension of the LOHC samples with dissolved H_2 up to T = 523 K in H_2 atmosphere up to 7 MPa indicated a slightly decreasing tendency with increasing p. Comparison of the results obtained for the reaction mixture and the binary mixture of the same degree of hydrogenation shows that the presence of H6-DPM does not influence interfacial tension and density significantly. With the successful application of the two experimental setups, a sound basis for further investigations of pure LOHC compounds and LOHC compound mixtures under the influence of H_2 and other gases has been established.

ACKNOWLEDGEMENTS

The authors gratefully acknowledge Holger Jorschick and Timo Rüde from the Helmholtz Institute Erlangen-Nürnberg for Renewable Energy, Forschungszentrum Jülich GmbH, for providing samples of H12-DPM as well as the reaction mixture.

FUNDING SOURCES

This work was funded by the Bavarian Ministry of Economic Affairs, Regional Development and Energy as well as by the German Research Foundation (Deutsche Forschungsgemeinschaft, DFG) through grant FR1709/15-1.

COMPETING INTERESTS STATEMENT

The authors declare that they have no competing interests.

SUPPORTING INFORMATION

The Supporting Information document related to this paper contains details on the experimental procedures of density measurements and their evaluation, tabulated density data measured at p = 0.1 MPa, the volume calibration and validation measurements related to the setup for solubility measurements, and the uncertainty analysis for interfacial tensions obtained with the new setup and the associated evaluation procedures.

REFERENCES

[1] Sartbaeva A, Kuznetsov VL, Wells SA, Edwards PP. Hydrogen nexus in a sustainable energy future. Energy Environ Sci 2008;1:79–85. https://doi.org/10.1039/b810104n.

[2] Teichmann D, Arlt W, Wasserscheid P, Freymann R. A future energy supply based on Liquid Organic Hydrogen Carriers (LOHC). Energy Environ Sci 2011;4:2767–73. https://doi.org/10.1039/c1ee01454d.

[3] Geburtig D, Preuster P, Bösmann A, Müller K, Wasserscheid P. Chemical utilization of hydrogen from fluctuating energy sources - Catalytic transfer hydrogenation from charged Liquid Organic Hydrogen Carrier systems. Int J Hydrogen Energy 2016;41:1010–7. https://doi.org/10.1016/j.ijhydene.2015.10.013.

[4] Teichmann D, Arlt W, Wasserscheid P. Liquid Organic Hydrogen Carriers as an efficient vector for the transport and storage of renewable energy. Int J Hydrogen Energy 2012;37:18118–32. https://doi.org/10.1016/j.ijhydene.2012.08.066.

[5] Abe JO, Popoola API, Ajenifuja E, Popoola OM. Hydrogen energy, economy and storage: Review and recommendation. Int J Hydrogen Energy 2019;44:15072–86. https://doi.org/10.1016/j.ijhydene.2019.04.068.

[6] Markiewicz M, Zhang YQ, Bösmann A, Brückner N, Thöming J, Wasserscheid P, Stolte S. Environmental and health impact assessment of Liquid Organic Hydrogen Carrier (LOHC) systems - challenges and preliminary results. Energy Environ Sci 2015;8:1035–45. https://doi.org/10.1039/c4ee03528c.

[7] Modisha PM, Ouma CNM, Garidzirai R, Wasserscheid P, Bessarabov D. The Prospect of Hydrogen Storage Using Liquid Organic Hydrogen Carriers. Energy and Fuels 2019;33:2778–96. https://doi.org/10.1021/acs.energyfuels.9b00296.

[8] Niermann M, Beckendorff A, Kaltschmitt M, Bonhoff K. Liquid Organic Hydrogen Carrier (LOHC) – Assessment based on chemical and economic properties. Int J Hydrogen Energy 2019;44:6631–54. https://doi.org/10.1016/j.ijhydene.2019.01.199.

[9] Aaldto-Saksa PT, Cook C, Kiviaho J, Repo T. Liquid organic hydrogen carriers for transportation and storing of renewable energy – Review and discussion. J Power Sources 2018;396:803–23. https://doi.org/10.1016/j.jpowsour.2018.04.011.

[10] Rao PC, Yoon M. Potential Liquid-Organic Hydrogen Carrier (LOHC) systems: A review on recent progress. Energies 2020;13:6040. https://doi.org/10.3390/en13226040.

[11] Leinweber A, Müller K. Solubility of Carbon Dioxide, Methane, and Nitrogen in Liquid Dibenzyl Toluene. J Chem Eng Data 2018;63:3527–33. https://doi.org/10.1021/acs.jced.8b00407.

[12] Wunsch A, Mohr M, Pfeifer P. Intensified LOHC-dehydrogenation using multi-stage microstructures and Pd-based membranes. Membranes (Basel) 2018;8. https://doi.org/10.3390/membranes8040112.

[13] Preuster P, Papp C, Wasserscheid P. Liquid organic hydrogen carriers (LOHCs): Toward

a hydrogen-free hydrogen economy. Acc Chem Res 2017;50:74–85. https://doi.org/10.1021/acs.accounts.6b00474.

[14] Aslam R, Müller K, Müller M, Koch M, Wasserscheid P, Arlt W. Measurement of Hydrogen Solubility in Potential Liquid Organic Hydrogen Carriers. J Chem Eng Data 2016;61:643–9. https://doi.org/10.1021/acs.jced.5b00789.

[15] Jorschick H, Bösmann A, Preuster P, Wasserscheid P. Charging a Liquid Organic Hydrogen Carrier System with H2/CO_2 Gas Mixtures. ChemCatChem 2018;10:4329–37. https://doi.org/10.1002/cctc.201800960.

[16] Tsuji T, Shinya Y, Hiaki T, Itoh N. Hydrogen solubility in a chemical hydrogen storage medium, aromatic hydrocarbon, cyclic hydrocarbon, and their mixture for fuel cell systems. Fluid Phase Equilib 2005;228–229:499–503. https://doi.org/10.1016/j.fluid.2004.07.013.

[17] Brunner E. Solubility of hydrogen in 10 organic solvents at 298.15, 323.15, and 373.15 K. J Chem Eng Data 1985;30:269–73. https://doi.org/10.1021/je00041a010.

[18] Zhou Z, Cheng Z, Yang D, Zhou X, Yuan W. Solubility of Hydrogen in Pyrolysis Gasoline. J Chem Eng Data 2006;51:972–6. https://doi.org/10.1021/je050478o.

[19] Stark K, Emel'yanenko VN, Zhabina AA, Varfolomeev MA, Verevkin SP, Müller K, Arlt W. Liquid Organic Hydrogen Carriers: Thermophysical and Thermochemical Studies of Carbazole Partly and Fully Hydrogenated Derivatives. Ind Eng Chem Res 2015;54:7953–66. https://doi.org/10.1021/acs.iecr.5b01841.

[20] Müller K, Stark K, Emel'yanenko VN, Varfolomeev MA, Zaitsau DH, Shoifet E, Schick C, Verevkin SP, Arlt W. Liquid Organic Hydrogen Carriers: Thermophysical and Thermochemical Studies of Benzyl- and Dibenzyl-toluene Derivatives. Ind Eng Chem Res 2015;54:7967–76. https://doi.org/10.1021/acs.iecr.5b01840.

[21] Aslam R, Khan MH, Ishaq M, Müller K. Thermophysical Studies of Dibenzyltoluene and Its Partially and Fully Hydrogenated Derivatives. J Chem Eng Data 2018;63:4580–7. https://doi.org/10.1021/acs.jced.8b00652.

[22] Müller K, Aslam R, Fischer A, Stark K, Wasserscheid P, Arlt W. Experimental

assessment of the degree of hydrogen loading for the dibenzyl toluene based LOHC system. Int J Hydrogen Energy 2016;41:22097–103. https://doi.org/10.1016/j.ijhydene.2016.09.196.

[23] Součková M, Klomfar J, Pátek J. Standard reference data for the air–liquid and vapor–liquid surface tension of benzene. Fluid Phase Equilib 2013;356:329–37. https://doi.org/10.1016/j.fluid.2013.07.053.

[24] Kahl H, Wadewitz T, Winkelmann J. Surface Tension and Interfacial Tension of Binary Organic Liquid Mixtures. J Chem Eng Data 2003;48:1500–7. https://doi.org/10.1021/je034062r.

[25] Kahl H, Wadewitz T, Winkelmann J. Surface Tension of Pure Liquids and Binary Liquid Mixtures. J Chem Eng Data 2003;48:580–6. https://doi.org/10.1021/je0201323.

[26] Hales J., Townsend R. Liquid densities from 293 to 490 K of nine aromatic hydrocarbons. J Chem Thermodyn 1972;4:763–72. https://doi.org/10.1016/0021-9614(72)90050-X.

[27] Zhang C, Li G, Yue L, Guo Y, Fang W. Densities, Viscosities, Refractive Indices, and Surface Tensions of Binary Mixtures of 2,2,4-Trimethylpentane with Several Alkylated Cyclohexanes from (293.15 to 343.15) K. J Chem Eng Data 2015;60:2541–8. https://doi.org/10.1021/acs.jced.5b00105.

[28] Christopher PM, Laukhuf WLS, Plank CA. The densities of methylcyclohexane-*n*-heptane mixtures. J Chem Eng Data 1976;21:443–5. https://doi.org/10.1021/je60071a013.

[29] Fröba AP, Leipertz A. Accurate Determination of Liquid Viscosity and Surface Tension Using Surface Light Scattering (SLS): Toluene under Saturation Conditions between 260 and 380 K. Int J Thermophys 2003;24:895–921. https://doi.org/10.1023/A:1025097311041.

[30] McLinden MO, Splett JD. A liquid density standard over wide ranges of temperature and pressure based on toluene. J Res Natl Inst Stand Technol 2008;113:29. https://doi.org/10.6028/jres.113.005.

[31] Baylaucq A, Boned C, Dauge P, Lagourette B. Measurements of the viscosity and density of three hydrocarbons and the three associated binary mixtures versus pressure and

temperature. Int J Thermophys 1997;18:3–23. https://doi.org/10.1007/BF02575198.

[32] Zéberg-Mikkelsen CK, Barrouhou M, Baylaucq A, Boned C. Viscosity and Density Measurements of Binary Mixtures Composed of Methylcyclohexane + cis-Decalin Versus Temperature and Pressure. Int J Thermophys 2003;24:361–74. https://doi.org/10.1023/A:1022911703225.

[33] Brückner N, Obesser K, Bösmann A, Teichmann D, Arlt W, Dungs J, Wasserscheid P. Evaluation of industrially applied heat-transfer fluids as liquid organic hydrogen carrier systems. ChemSusChem 2014;7:229–35. https://doi.org/10.1002/cssc.201300426.

[34] Jorschick H, Geißelbrecht M, Eßl M, Preuster P, Bösmann A, Wasserscheid P. Benzyltoluene/dibenzyltoluene-based mixtures as suitable liquid organic hydrogen carrier systems for low temperature applications. Int J Hydrogen Energy 2020;45:14897–906. https://doi.org/10.1016/j.ijhydene.2020.03.210.

[35] Kerscher M, Klein T, Schulz PS, Veroutis E, Dürr S, Preuster P, Koller TM, Rausch MH, Economou IG, Wasserscheid P, Fröba AP. Thermophysical properties of diphenylmethane and dicyclohexylmethane as a reference liquid organic hydrogen carrier system from experiments and molecular simulations. Int J Hydrogen Energy 2020;45:28903-19. https://doi.org/10.1016/j.ijhydene.2020.07.261.

[36] Rivard E, Trudeau M, Zaghib K. Hydrogen storage for mobility: A review. Materials 2019;12:1973. https://doi.org/10.3390/ma12121973.

[37] Lemmon EW, Bell IH, Huber ML, McLinden MO. NIST Standard Reference Database 23: Reference Fluid Thermodynamic and Transport Properties - REFPROP, Version 10.0, National Institute of Standards and Technology 2018. https://doi.org/https://dx.doi.org/10.18434/T4JS3C.

[38] Sigma-Aldrich. Safety data sheet for diphenylmethane. Product number D209317, revision date 17. September 2019 n.d. https://www.sigmaaldrich.com/MSDS/MSDS/PleaseWaitMSDSPage.do?language=EN-generic&country=DE&brand=ALDRICH&productNumber=D209317&PageToGoToURL=https%253A%252F%252Fwww.sigmaaldrich.com%252Fcatalog%252Fsearch%253Fter

m%253Ddiphenylmethane%2526interface%253DAl (accessed March 08, 2021).

[39] Han DJ, Jo YS, Shin BS, Jang M, Kang JW, Han JH, Nam SW, Yoon CW. A Novel Eutectic Mixture of Biphenyl and Diphenylmethane as a Potential Liquid Organic Hydrogen Carrier: Catalytic Hydrogenation. Energy Technol 2019;7:113–21. https://doi.org/10.1002/ente.201700694.

[40] Jang M, Jo YS, Lee WJ, Shin BS, Sohn H, Jeong H, Jang SC, Kwak SK, Kang JW, Yoon CW. A High-Capacity, Reversible Liquid Organic Hydrogen Carrier: H_2-Release Properties and an Application to a Fuel Cell. ACS Sustain Chem Eng 2019;7:1185–94. https://doi.org/10.1021/acssuschemeng.8b04835.

[41] Kwak Y, Moon S, Ahn C-i, Kim A-R, Park Y, Kim Y, Sohn H, Jeong H, Nam SW, Yoon CW, Jo YS. Effect of the support properties in dehydrogenation of biphenyl-based eutectic mixture as liquid organic hydrogen carrier (LOHC) over Pt/Al_2O_3 catalysts. Fuel 2021;284:119285. https://doi.org/10.1016/j.fuel.2020.119285.

[42] Chang JS, Lee MJ, Lin HM. Densities of *m*-Xylene + Diphenylmethane and *m*-Cresol + Diphenylmethane from 333 K to 413 K and Pressures up to 30 MPa. J Chem Eng Data 1997;42:574–9. https://doi.org/10.1021/je960334x.

[43] Koefoed J, Villadsen J V. Surface Tension of Liquid Mixtures. A Micro-Method Applied to the Systems: Chloroform-Carbon-tetrachloride, Benzene-Diphenylmethane, and Heptane-Hexadecane. Acta Chem Scand 1958;12:1124–35. https://doi.org/10.3891/acta.chem.scand.12-1124.

[44] Harkins WD, Ewing DT. The effects of acids and bases on the surface energy relations of *β*,*β*-dichloroethyl-sulfide (“Mustard gas”). J Am Chem Soc 1919;41:1977–80. https://doi.org/10.1021/ja02233a014.

[45] Cukor PM, Prausnitz JM. Solubilities of gases in liquids at elevated temperatures. Henry’s constants for hydrogen, methane, and ethane in hexadecane, bicyclohexyl, and diphenylmethane. J Phys Chem 1972;76:598–601. https://doi.org/10.1021/j100648a026.

[46] Simnick JJ, Liu KD, Lin HM, Chao KC. Gas-Liquid Equilibrium in Mixtures of Hydrogen and Diphenylmethane. Ind Eng Chem Process Des Dev 1978;17:204–8.

https://doi.org/10.1021/i260066a015.

[47] May EF, Tay WJ, Nania M, Aleji A, Al-Ghafri S, Martin Trusler JP. Physical apparatus parameters and model for vibrating tube densimeters at pressures to 140 MPa and temperatures to 473 K. Rev Sci Instrum 2014;85:095111. https://doi.org/10.1063/1.4894469.

[48] Lei Z, Dai C, Chen B. Gas solubility in ionic liquids. Chem Rev 2014;114:1289–326. https://doi.org/10.1021/cr300497a.

[49] Leachman JW, Jacobsen RT, Penoncello SG, Lemmon EW. Fundamental Equations of State for Parahydrogen, Normal Hydrogen, and Orthohydrogen. J Phys Chem Ref Data 2009;38:721–48. https://doi.org/10.1063/1.3160306.

[50] Wieczorek SA, Kobayashi R. Vapor pressure measurements of diphenylmethane, thianaphthene, and bicyclohexyl at elevated temperatures. J Chem Eng Data 1980;25:302–5. https://doi.org/10.1021/je60087a010.

[51] Grosse A V., Mavity JM, Mattox WJ. Catalytic Dehydrogenation of Polycyclic Naphthenes. Ind Eng Chem 1946;38:1041–5. https://doi.org/10.1021/ie50442a019.

[52] Smith HA, Alderman DM, Shacklett CD, Welch CM. The Catalytic Hydrogenation of the Benzene Nucleus. VI. The Hydrogenation of Compounds with Two Benzene Rings. J Am Chem Soc 1949;71:3772–6. https://doi.org/10.1021/ja01179a056.

[53] Serijan KT, Wise PH. Dicyclic Hydrocarbons. III. Diphenyl- and Dicyclohexylalkanes through C_{15}. J Am Chem Soc 1951;73:4766–9. https://doi.org/10.1021/ja01154a086.

[54] Wu W, Klein T, Kerscher M, Rausch MH, Koller TM, Giraudet C, Fröba AP. Mutual and Thermal Diffusivities as well as Fluid-Phase Equilibria of Mixtures of 1-Hexanol and Carbon Dioxide. J Phys Chem B 2020;124:2482–94. https://doi.org/10.1021/acs.jpcb.0c00646.

[55] Rusanov AI, Prokhorov VA. Interfacial Tensiometry. vol. 3. Amsterdam, New York: Elsevier; 1996.

[56] Young T. III. An essay on the cohesion of fluids. Philos Trans R Soc London 1805;95:65–

87. https://doi.org/10.1098/rstl.1805.0005.

[57] Laplace PS. Traité de mécanique céleste. Paris, France: Gauthier-Villars; 1805.

[58] Saad SMI, Neumann AW. Axisymmetric Drop Shape Analysis (ADSA): An Outline. Adv Colloid Interface Sci 2016;238:62–87. https://doi.org/10.1016/j.cis.2016.11.001.

[59] Rotenberg Y, Boruvka L, Neumann AW. Determination of surface tension and contact angle from the shapes of axisymmetric fluid interfaces. J Colloid Interface Sci 1983;93:169–83. https://doi.org/10.1016/0021-9797(83)90396-X.

[60] Hoorfar M, W. Neumann A. Recent progress in Axisymmetric Drop Shape Analysis (ADSA). Adv Colloid Interface Sci 2006;121:25–49. https://doi.org/10.1016/j.cis.2006.06.001.

[61] Canny J. A Computational Approach to Edge Detection. IEEE Trans Pattern Anal Mach Intell 1986;PAMI-8:679–98. https://doi.org/10.1109/TPAMI.1986.4767851.

[62] Runge C. Ueber die numerische Auflösung von Differentialgleichungen. Math Ann 1895;46:167–78. https://doi.org/10.1007/BF01446807.

[63] Kutta W. Beitrag zur näherungsweisen Integration totaler Differentialgleichungen. Z Math Phys 1901;46:435–53.

[64] Bucher I. Circle fit. MATLAB Central File Exchange 2004. https://de.mathworks.com/matlabcentral/fileexchange/5557-circle-fit (accessed October 12, 2020).

[65] Hansen F., Rødsrud G. Surface tension by pendant drop. J Colloid Interface Sci 1991;141:1–9. https://doi.org/10.1016/0021-9797(91)90296-K.

[66] Tegeler C, Span R, Wagner W. A New Equation of State for Argon Covering the Fluid Region for Temperatures From the Melting Line to 700 K at Pressures up to 1000 MPa. J Phys Chem Ref Data 1999;28:779–850. https://doi.org/10.1063/1.556037.

[67] Mulero A, Cachadiña I, Parra MI. Recommended Correlations for the Surface Tension of Common Fluids. J Phys Chem Ref Data 2012;41:043105. https://doi.org/10.1063/1.4768782.

[68] Huber ML. Models for viscosity, thermal conductivity, and surface tension of selected pure fluids as implemented in REFPROP v10.0. NIST Interagency/Internal Report (NISTIR) 2018;8209. https://doi.org/10.6028/NIST.IR.8209.

[69] Petrova T, Dooley RB. Revised Release on Surface Tension of Ordinary Water Substance. Moscow, Russia: The International Association for the Properties of Water and Steam; 2014.

[70] Rausch MH, Kretschmer L, Will S, Leipertz A, Fröba AP. Density, Surface Tension, and Kinematic Viscosity of Hydrofluoroethers HFE-7000, HFE-7100, HFE-7200, HFE-7300, and HFE-7500. J Chem Eng Data 2015;60:3759–65. https://doi.org/10.1021/acs.jced.5b00691.

[71] Hefter GT, Tomkins RPT, editors. The Experimental Determination of Solubilities. Chichester, UK: John Wiley & Sons, Ltd; 2003. https://doi.org/10.1002/0470867833.

[72] Dymond J, Hildebrand JH. Apparatus for Accurate, Rapid Determinations of Solubility of Gases in Liquids. Ind Eng Chem Fundam 1967;6:130–1. https://doi.org/10.1021/i160021a022.

[73] Berger Bioucas FE, Piszko M, Kerscher M, Preuster P, Rausch MH, Koller TM, Wasserscheid P, Fröba AP. Thermal Conductivity of Hydrocarbon Liquid Organic Hydrogen Carrier Systems: Measurement and Prediction. J Chem Eng Data 2020;65:5003–17. https://doi.org/10.1021/acs.jced.0c00613.